Chronic intermittent hypoxia impairs diuretic and natriuretic responses to volume expansion in rats with preserved low-pressure baroreflex control of the kidney

Sara AlMarabeh[a], Julie O'Neill[a], Jeremy Cavers[a], Eric F. Lucking[a], Ken D. O'Halloran[a], Mohammed H. Abdulla[a]

[a] *Department of Physiology, School of Medicine, College of Medicine and Health, University College Cork, Cork, Ireland*

Running Head: Intermittent hypoxia affects baroreflex and renal function

Word count: 9316 total article; 6266 (Introduction to Discussion).

Number of tables: 4 (and 3 supplementary tables)

Number of figures: 9

Correspondence: Mohammed H. Abdulla, Department of Physiology, University College Cork, Western Gateway Building, Western Road, Cork, Ireland. Email: m.abdulla@ucc.ie

Supplementary material available at:

URL: https://figshare.com/s/7bc496e361e5e47043d7; DOI: 10.6084/m9.figshare.12937433
URL: https://figshare.com/s/7796b802afe6c02d54f0; DOI: 10.6084/m9.figshare.12937571
URL: https://figshare.com/s/870e5f260f49995a4d8d; DOI: 10.6084/m9.figshare.12937580
URL: https://figshare.com/s/9659e62049b971e25ab7; DOI: 10.6084/m9.figshare.12937373

Abstract

We examined the effects of exposure to chronic intermittent hypoxia (CIH) on baroreflex control of renal sympathetic nerve activity (RSNA) and renal excretory responses to volume expansion (VE) before and after intra-renal TRPV1 blockade by capsaizepine (CPZ). Male Wistar rats were exposed to 96 cycles of hypoxia per day for 14 days (CIH), or normoxia. Urine flow and absolute Na^+ excretion during VE were less in CIH-exposed rats, but the progressive decrease in RSNA during VE was preserved. Assessment of the high-pressure baroreflex revealed an increase in the operating and response range of RSNA and decreased slope in CIH-exposed rats with substantial hypertension (+19mmHg basal mean arterial pressure, MAP), but not in a second cohort with modest hypertension (+12mmHg). Intra-renal CPZ caused diuresis, natriuresis and a reduction in MAP in sham and CIH-exposed rats. Following intra-renal CPZ, diuretic and natriuretic responses to VE in CIH-exposed rats were equivalent to sham. TPRV1 expression in the renal pelvic wall was similar in both experimental groups. Exposure to CIH did not elicit glomerular hypertrophy, renal inflammation or oxidative stress. We conclude that exposure to CIH: 1) does not impair the low-pressure baroreflex control of RSNA; 2) has modest effects on the high-pressure baroreflex control of RSNA, most likely indirectly due to hypertension; 3) can elicit hypertension in the absence of kidney injury; and 4) impairs diuretic and natriuretic responses to fluid overload. Our results suggest that exposure to CIH causes renal dysfunction, which may be relevant to obstructive sleep apnea.

Key words: Intermittent hypoxia, baroreflex, volume expansion, diuresis, TPRV1.

Abbreviations:

ADH	Anti-diuretic hormone
ANP	Atrial natriuretic peptide
AOPP	Advanced Oxidation Protein Products
AUC	Area under curve
CGRP	Calcitonin gene- related peptide
CIH	Chronic intermittent hypoxia
CPZ	Capsaizepine
DBP	Diastolic blood pressure
GFR	Glomerular filtration rate
HR	Heart rate
MAP	Mean arterial blood pressure
NOX	NADPH oxidase
OSA	Obstructive sleep apnea
ROS	Reactive oxygen species
RSNA	Renal sympathetic nerve activity
SBP	Systolic blood pressure
SOD	Superoxide dismutase
SP	Substance P
TRPV1	Transient receptor potential cation channel subfamily V member 1
UFR	Urine flow rate
VE	Volume expansion
IFN-Ɣ	Interferon gamma
IL-1β	Interleukin 1 beta
IL-4	Interleukin 4
TNF-α	Tumor necrosis factor alpha

Introduction

Obstructive sleep apnea (OSA) syndrome is characterized by frequent interruption of ventilation due to repetitive upper airway obstruction during sleep (35). People with OSA have a three-fold higher risk of developing hypertension (1). Chronic intermittent hypoxia (CIH) models the hypoxia and reoxygenation cycles experienced in OSA, due to recurrent apnea. There is evidence from studies in animal models and humans (25) that exposure to IH elicits sympatho-excitation and hypertension, revealing that this characteristic feature of the disorder is adequate to cause autonomic dysfunction, notwithstanding that other features of OSA, not modelled in CIH, such as hypercapnia and large intra-thoracic sub-atmospheric pressure swings associated with airway obstruction, could also contribute to cardiovascular dysfunction in OSA. Animal models of CIH develop sympathetic hyperactivity and diurnal hypertension (28, 40, 41, 51). Moreover, exposure to CIH evokes detrimental processes in the kidney such as inflammation, fibrosis, glomerulosclerosis and proteinuria (4, 5, 29, 45), which are markers for chronic kidney disease.

Fluid homeostasis is mainly regulated by the diuretic and natriuretic function of the kidney. Fluid overload activates low-pressure cardiopulmonary baroreceptors causing a reflex suppression of renal sympathetic nerve activity (RSNA) promoting natriuresis and diuresis (33, 37). Previous studies have revealed blunted low-pressure baroreflex control of RSNA in response to fluid overload in disease models that involve kidney injury (3, 19, 20). Indeed, failure of the baroreflex mechanism is associated with long-term elevation of sympathetic nerve activity, which initiates and/or exacerbates hypertension (15). The influence of exposure to CIH on the low-pressure baroreflex control of RSNA and kidney function has not yet been examined. In addition, there is little known about the effects of exposure to CIH on the high-pressure baroreflex control of RSNA.

The importance of renal innervation in long-term control of blood pressure has received attention following clinical trials showing that bilateral renal denervation was associated with a significant reduction of blood pressure in people who are hypertensive with OSA (16, 43, 49). The involvement of renal nerves in mediating the derangement of baroreflex control of blood pressure is revealed by renal denervation, which restored the sensitivity of blunted high- and low-pressure baroreflex control of RSNA in models of hypertension that involve renal injury (19). In addition, pharmacological inhibition of renal

86 inflammation, a feature of animal models of CIH (29, 45, 46, 48), was associated with
87 normalization of baroreflex control of RSNA (3, 21).

88 Previous studies have shown that selective renal deafferentation was associated with
89 attenuation of the hypertensive phenotype (9, 12). Afferent renal nerves are densely located
90 in the renal pelvic wall and to a lesser extent in the cortex, and their activity is mediated by
91 the neuropeptides, calcitonin gene related peptide (CGRP) and substance P (SP) (13, 30). SP
92 release is modulated by the activity of other receptors, such as transient receptor potential
93 vanilloid 1 (TRPV1) channels, localized in the renal pelvic wall. TRPV1 receptors are non-
94 selective cation channels that allow the influx of Na^{+}, Mg^{2+} and Ca^{2+} (17). Renal TRPV1
95 activation is associated with an increase in RSNA and blood pressure in rats (10, 36). In
96 addition, acute hypoxia increases basal TRPV1 outward current amplitudes, which is
97 suggested to be due to increased intracellular reactive oxygen species (ROS), that can
98 increase intracellular Ca^{2+}, with excitatory effects on the afferent reflex (10, 22). Thus,
99 exposure to CIH might provoke renal oxidative stress and inflammation, sufficient to activate
100 renal afferent discharge via TRPV1 receptors, eliciting excitatory reno-renal reflexes
101 contributing to hypertension.

102 The current study was designed to examine the effects of exposure to CIH on high-
103 and low-pressure baroreflex control of RSNA and renal excretory responses to fluid overload.
104 We hypothesized that exposure to CIH increases TRPV1 signalling via renal afferent nerves
105 modulating baroreflex control of RSNA. We examined high- and low-pressure baroreflexes
106 and renal diuretic and natriuretic responses to fluid overload in control and CIH-exposed rats,
107 before and after intra-renal TRPV1 blockade with capsaizepine (CPZ).

108

109

Materials and Methods

Ethical approval

Eight-week old male Wistar rats were purchased from Envigo (Bicester, UK) and were housed in our institution's animal facility under 12-hour light: 12-hour dark cycle with water and standard chow available *ad libitum*. All experimental procedures were conducted under authorization from the Health Products Regulatory Authority [AE19130/P073] in accordance with European Union directive (2010/63/EU) with prior ethical approval from University College Cork (AEEC 2018/002).

Animal model of chronic intermittent hypoxia

Rats were randomly divided into two experimental groups: CIH and sham (control). Rats assigned to the CIH group were placed in commercial environmental chambers attached to a computer-controlled gas delivery system (Oxycycler™, Biospherix, NY, USA). Rats in the CIH group were exposed to recurrent hypoxia cycles, resulting in changes in ambient oxygen concentration every 5 min within the chamber from 21±2% for 210 sec to a nadir value of 6±0.5% over 90 sec), for 12 cycles per hour, for 8h during the daytime (lights on), for 14 consecutive days. Rats of the sham group were housed in the same room and were exposed to ambient air (~21% O_2) for 14 days. On day 15, rats were prepared surgically to assess high- and low-pressure baroreflexes under anesthesia.

Surgical protocol

CIH-exposed (n=20) and sham rats (n=23) were anesthetized by intra-peritoneal injection of a mixture of urethane (416 mg/kg, Sigma-Aldrich, St. Louis, MO, USA), α-chloralose (27 mg/kg, Sigma-Aldrich) and sodium pentobarbital (Euthatal (200 mg/ml), Merial animal health Ltd, UK, 33 mg/kg). Anesthesia was maintained during surgery using a maintenance dose of a mixture of urethane (62 mg/kg) and α-chloralose (4 mg/kg), given as intravenous bolus injection. Animals were placed on a temperature-controlled heating pad to maintain body temperature at 37°C (Harvard Apparatus, Cambridge, UK). Airway patency was facilitated by tracheotomy (PE240, Portex, Kent, UK). A cannula (PE25 attached to PE50) containing heparinized saline (4 U/ml), connected to a fluid-filled pressure transducer

(ADInstruments, Hastings, UK) was inserted into the right femoral artery to measure arterial blood pressure and heart rate (HR). The pressure transducer was connected to a quad-bridge amplifier that recorded pulsatile blood pressure using LabChart 7 software (ADInstruments, Oxford, UK). The right femoral vein was cannulated (PE50) to infuse FITC-inulin (10 mg/kg/hr, TdB consultancy, Uppsala, Sweden) continuously over the duration of the experiment (32). The urinary bladder was cannulated (PE240) to collect urine samples.

Baseline blood pressure was recorded for 2 minutes ~4-5 minutes after femoral artery cannulation (before surgical access of the kidney) and compared between the groups, in essence to confirm the hypertensive phenotype in CIH-exposed rats. In the first of the two cohort studies, CIH-exposed (n=9) and sham animals (n=10) were then placed on their right side and the left kidney was exposed by a retroperitoneal flank incision. A cannula (PE10) was inserted into the rostral part of the left kidney at 3.5-4.5 mm depth, to reach the cortico-medullary region of the kidney (3) and was fixed in place using acrylate glue. This cannula was connected to a 25 µl micro-syringe (Hamilton, USA) placed on a micro-infusion pump (KD Scientific, Linton Instruments, Norfolk, UK) to infuse saline or CPZ (5 µg/ml, Sigma-Aldrich, St. Louis, MO, USA) at 17 µl/min. In the second cohort study, CIH-exposed (n=10) and sham rats (n=13) were placed on their left side to expose the right kidney, which was cannulated using a similar approach to the first cohort.

In both cohorts, the renal nerve bundle running between the renal artery and vein of the left kidney was dissected and placed on a bipolar multi-stranded stainless-steel electrode (Medwire, NY, USA). The nerve bundle was sealed over the recording electrode using silicone glue (Klasse 4 dental, Augsburg, Germany). RSNA was recorded using a high impedance head stage attached to an amplifier (NeuroAMP EX®, ADInstruments, UK) connected to a Power Lab data acquisition system.

Experimental protocol

The experimental protocol of the first cohort study is described in Figure 1. Baseline MAP, HR and RSNA were recorded. After intra-renal infusion of saline to the left kidney high-pressure baroreflex responses were determined. Successive volume expansion (VE) challenges were performed, first during intra-renal infusion of saline and then during intra-renal infusion of the TRPV1 blocker, CPZ.

The animals were euthanized at the end of the experiment by an overdose of anaesthetic (mixture of 80 g/kg urethane and 55 mg/kg α-chloralose), given intravenously. RSNA reaches its maximum level during euthanasia due to the sudden precipitous drop of blood pressure, before the complete disappearance of RSNA. The maximum RSNA was determined to allow normalization of baseline RSNA to the maximum. The minimum electrical activity was measured to determine background noise, which was subtracted from all recordings.

The second cohort study involved exclusive assessment of the high-pressure baroreflex response CIH-exposed (n=10) and sham rats (n=10) during two successive phases. The first phase was after 30 minutes of intra-renal infusion of saline (17 µl/min) and the second phase was after 30 minutes of intra-renal infusion of CPZ (5 µg/ml at 17 µl/min). In this cohort of rats, neither VE challenges nor renal function measurements were performed.

Measurement of Excretory Parameters

Blood samples (P1-P3 samples, Figure 1) of ~400 µl were collected and underwent centrifugation at 10,956 *g* for 1 minute. Plasma was stored at -20° for further analysis. To minimise any change in hematocrit, the blood cells that remained after centrifugation were suspended in an equivalent volume of saline and returned to the animal via the arterial line. Blood samples (at P1 and P3, Figure 1) were taken from the femoral artery to measure sodium concentration using an i-STAT system (Abbott Laboratories, penAbbott Park, IL, USA). Two urine samples were collected (U1 and U2, Figure 1), during intra-renal infusion of saline or CPZ. In addition, urine samples were collected during VE (Figure 1). An additional urine sample was collected during the recovery period i.e. 30 minutes after the end of the VE trial (Figure 1).

Urine flow (UF), glomerular filtration rate (GFR), and absolute and fractional Na^+ excretion were measured at baseline and during the VE trial. Urine volume was measured gravimetrically and UF was calculated as: UF = Uv/t; *Uv* is urine volume, *t* is time of urine collection. GFR was measured as a function of FITC-inulin clearance and was calculated using the formula: GFR= ([Uin]Uv)/[Pin]; *[Uin]* is urine concentration of FITC-inulin, *[Pin]* is plasma concentration of FITC-inulin. FITC-fluorescence was measured in urine and plasma samples using a fluorometric microplate reader (Wallac victor^2 1420 multilabel counter, Perkin Elmer, MA, USA). Urinary Na^+ concentration was measured using flame

photometry (M410, Sherwood Scientific, Cambridge, UK). Plasma Na^+ concentration at P2 was determined using flame photometry. However, plasma Na^+ concentration (P1 and P3) was measured immediately upon sample collection using the i-STAT system. Absolute Na^+ excretion was calculated using the formula: [UNa^+]. UF; *[UNa^+]* is urinary Na^+ concentration. Fractional Na^+ excretion was calculated using the equation: Na^+ clearance/GFR.100% where *Na^+ clearance = ([UNa^+]Uv)/[PNa^+]; [PNa^+]* is plasma Na^+ concentration.

Atrial natriuretic peptide assay

Atrial natriuretic peptide (ANP) was quantified in plasma samples at baseline (P2) and during VE (P3) of the saline phase in CIH-exposed (n=7) and sham rats (n=7) using a quantitative sandwich ELISA kit (My BioSource, San Diego, CA, USA) as per the manufacturer's instructions.

Tissue preparation

In separate studies, male Wistar rats were exposed for 14 days to normoxia or CIH as described previously. On day 15, rats were euthanized by an overdose of sodium pentobarbital (Dolethal (200 mg/ml), Vetoquinol, France, 60 mg/kg), given intra-peritoneally. The left kidney was collected and halved along its sagittal plane. Each half was cut transversely into three sections: top, middle (containing the pelvic wall) and bottom. Sections were preserved at -80^{o}C for later use. Immediately after harvesting the left kidney, the left renal artery and vein were closed by a bulldog clamp. Intra-cardiac puncture via the left ventricle was performed and warmed heparinized saline (~ 63 U/ml) was infused. The rate of infusion was 35 ml/min, which was raised gradually to 60 ml/min until 250-300 ml of heparinized saline was infused into each animal. This was followed by infusion of 4% paraformaldehyde at an infusion rate of 60 ml/min (Formalin solution, neutral buffered, 10%, Sigma-Aldrich, St. Louis, MO, USA). The upper and lower poles of the right kidney were removed, and the remnant kidney was either post-fixed for 24 hours for studies employing immunofluorescence techniques, or wax-embedded in paraffin. Some kidneys that were harvested from sham and CIH-exposed rats that underwent surgical procedures were also perfusion-fixed and wax-embedded in paraffin. In separate CIH-exposed (n=6) and sham rats

(n=6) that were not perfusion-fixed, the right kidneys were excised and after removal of the upper and lower poles, were directly post-fixed in formalin solution for 24 hours for subsequent use in studies employing immunofluorescence techniques.

Biochemical assays

The middle part of the left kidney was homogenized (32) for use in different assays: Advanced Oxidation Protein Products (AOPP) assay (Cell Biolabs, San Diego, CA), superoxide dismutase (SOD) and catalase activity assays (Cayman Chemical, Ann Arbor, MI, USA) and a TRPV1 ELISA assay (Mybiosource, Tokyo, Japan) (sham, n=12; CIH, n=8). The same homogenization protocol (32) was used to prepare samples for the assessment of NADPH oxidase (NOX) activity (39) and to determine the concentrations of inflammatory cytokines in renal tissue (sham, n=11; CIH, n=10), except for the use of a lysis buffer made of Tris-HCL (20 mM, pH 7.5, Sigma-Aldrich), sodium chloride (150 mM) and 1% Triton-X-100 (Molekula, Dorset, UK) instead of RIPA during homogenization. Absorbances were measured using a microplate reader (SpectraMax® M3, molecular devices, California, USA).

Renal inflammatory cytokines

Pro-inflammatory and anti-inflammatory cytokines (IFN-γ, IL-1β, IL-4, IL-5, IL-6, keratinocyte chemoattractant/growth related oncogene, IL-10, IL-13, and TNF-α) were analysed by sandwich immunoassay using a V-plex proinflammatory panel 2 rat kit (Meso Scale Discovery, Rockville, MD, USA), as per the manufacturer's instructions. Plates were analysed using a QuickPlex SQ 120 plate reader (Meso Scale Discovery). IL-1β, TNF-α and keratinocyte chemoattractant/growth related oncogene were successfully measured. The concentration of all other cytokines in kidney were below the detection limits of the kit.

Immunofluorescence

Immunofluorescence for TRPV1 protein expression in the renal pelvic wall was carried out on 3 CIH-exposed and 3 sham kidneys that were perfusion-fixed and post-fixed, in addition to 6 CIH-exposed and 5 sham kidneys that were only post-fixed. Frozen, formalin-fixed kidneys were sectioned to 20 μm sagittal sections using a cryostat (Leica

Biosystems, Wetzlar, Germany). Three sections that contained the renal pelvic wall were randomly selected from each kidney by systematic random sampling. Non-specific binding was blocked by incubating sections in 5% goat serum and 1% bovine serum albumin (with 0.5% triton-X) for one hour. Then, sections were incubated with rabbit polyclonal anti-TRPV1 antibody (1:200, ACC-030, Alomone labs) diluted with 5% goat serum, 1% bovine serum albumin and 0.5% triton-X for two hours at 37°C. Sections were incubated with goat anti-rabbit FITC secondary antibody (1:100, Sigma-Aldrich, St. Louis, MO, USA) for two hours at room temperature. Sections were covered with anti-fade mounting medium (Vectashield, Vector laboratories, Burlingame, CA, USA).

Images were captured using a laser scanning confocal microscope (Olympus FV1000-IX71, Tokyo, Japan) provided with filters for FITC and DAPI. Sections were initially visualized using 20X magnification under the DAPI filter and three regions of the pelvic wall were randomly selected from each section. After selection, the FITC filter was switched on to capture images. Positive staining was detected in the uroepithelial layer and submucosa/ muscularis propria layers of the pelvic wall. Images were transferred to black and white images and the threshold was adjusted to highlight the area occupied by fluorescent labeling of TRPV1 using Image J software. Threshold area was calculated and normalized to the total area of the uroepithelium within the image to quantify the expression of TPRV1 in that region. Similarly, threshold area in the submucosa and muscularis propria layers were calculated and normalized to the total area identified in the image.

Renal histopathological staining

Kidneys were taken from CIH-exposed (n=8) and sham rats (n=8) that underwent surgical procedures as well as from rats euthanized following exposure to gasses without undergoing surgery. Paraffin blocks were cut to 10 μm tissue sections using a rotary microtome (Leica RM2135, Germany). Two sections were randomly selected by random number generator each from the upper, middle and bottom parts of the paraffin block (a total of 6 sections from each kidney block). Sections were de-waxed using Neo-Clear® xylene substitute (Merck, Darmstadt, Germany) and washed with down-graded levels of ethanol. Tissue sections were then stained in hematoxylin (Hematoxylin Solution, Harris Modified, Sigma-Aldrich, St. Louis, MO, USA) and eosin (Surgipath Europe LTD, Cambridgeshire, UK or with Sirius red stain (0.1% Direct red 80, Sigma-Aldrich, India). Sections were cleared

296 in Neo-Clear® xylene substitute, and mounted with DPX mounting medium (Sigma-Aldrich,
297 St. Louis, MO, USA).

298 Hematoxylin and Eosin staining was used to examine total glomerular tuft area. A
299 virtual grid comprised of 91 squares was created to enable random sampling of cortical areas
300 of each kidney section. Selected squares were magnified using a 40X magnification lens to
301 image selected glomeruli (only when the juxtaglomerular apparatus was evident). As some
302 squares did not include any glomeruli and/or the juxtaglomerular apparatus was not visible in
303 some glomeruli, other squares were randomly chosen so that a total of 3 glomeruli per kidney
304 section were analyzed. As 6 sections were randomly selected from each animal, a total of 18
305 glomeruli per animal were chosen to measure glomerular tuft area. Images were taken using a
306 40X magnification lens (Olympus inverted BX53F microscope, Tokyo, Japan) and tuft area
307 was measured using ImageJ software.

308 Sirius red stain was used to semi-quantify areas occupied by collagen in the cortex
309 and outer medulla. A virtual grid with 25 squares was used to enable random selection of
310 cortical and medullary areas. Selected squares were magnified using a 20X magnification
311 lens to capture images. Three cortical areas and two outer medullary areas per kidney section
312 were randomly chosen. As 6 sections were stained from each animal, a total of 18 cortical
313 areas and 12 areas from the outer medulla were selected for analysis. Glomeruli and
314 perivascular fibres were omitted from images before analysis. The fibrotic area of each image
315 was normalized to the total area of the captured image to generate the % fibrotic area (Figure
316 2).

317 *Statistical analysis*

318 Data in tables and within text are presented as mean ± SD. Line figures are shown as
319 mean ± SE. Baseline MAP, HR and RSNA were compared between groups using
320 independent sample *t*-tests. Baseline RSNA was expressed as absolute values (μV.s) and also
321 was normalized to the maximum RSNA value recorded during euthanasia, expressed as
322 RSNA (% of max). Values were compared between groups using repeated-measures two-way
323 ANOVA.

324 Baseline values for UF, GFR, and absolute and fractional Na^+ excretion were
325 compared using repeated-measures two-way ANOVA. RSNA sympatho-inhibitory response
326 to VE was expressed as % of baseline (baseline=100%) and as RSNA (% of max). The
327 change in functional parameters and the decrease in RSNA in response to VE were analysed

using repeated-measures two-way ANOVA followed by a Bonferroni *post hoc* test. The area under the curve (AUC) of RSNA (% of baseline), RSNA (% of max), and each functional parameter was compared between groups and between the saline VE phase and CPZ VE phase using independent sample *t*-test and paired *t*-test, with significance taken at $P<0.0125$, accounting for multiple comparisons.

High pressure baroreflex function curves were fitted according to a logistic sigmoidal function equation that shows the relationship between MAP and RSNA or HR [$y=A1/(1+\exp(A2(x-A3)))+A4$] where y is the RSNA or HR; A1, response range over which baroreceptors operate; A2, gain coefficient; A3, mid-point blood pressure; A4, minimum response of RSNA or HR. Parameters were compared between the sham and CIH-exposed groups using independent sample *t*-test and significance was taken at $P<0.05$.Baroreflex gain curve parameters during the first (saline) and second (CPZ) phase were compared using paired *t*-tests. Significance was taken at $P<0.0125$, accounting for multiple comparisons.

Data from biochemical assays, histology and immunofluorescence from CIH-exposed and sham tissues were analysed using independent sample *t*-tests or Mann-Whitney tests, and significance was taken at $P<0.05$. All statistical analyses were performed using SPSS software (SPSS Statistics for Windows, v25.0. IBM corp., NY, USA). All graphs were plotted using GraphPad® Prism (v6, GraphPad software, San Diego, CA, USA).

Results

Baseline MAP, HR, RSNA and renal excretory parameters

A representative recording of baseline parameters is shown in Figure 3. In the first cohort study, MAP was greater in CIH-exposed rats compared with sham rats (Table 1). Baseline RSNA was greater in CIH-exposed rats compared with sham rats (RSNA (% of max), 36±15% vs. 17±7%, p=0.006). MAP was greater in CIH-exposed rats of the second cohort compared with sham rats, but to a lesser extent compared with rats of the first cohort study (Table 1 and Supplementary Table 1 https://figshare.com/s/7bc496e361e5e47043d7). HR was similar in CIH-exposed and sham rats of both cohorts. Baseline renal function data are shown in Supplementary Table 2 (https://figshare.com/s/7796b802afe6c02d54f0). Exposure to CIH had no significant effect on any of the basal renal excretory parameters.

Cardiovascular responses to VE

Baseline ANP concentration in plasma prior to VE challenge was not significantly different between CIH-exposed and sham rats (CIH vs. sham; 157±17 vs. 167±36 pg/ml). MAP and HR data during each VE trial are shown in Figure 4a and 4b. During the last 2 minutes of each VE trial, MAP was not significantly different from respective baseline values recorded prior to VE (Table 2). HR was significantly elevated during the last 2 minutes of each of the VE trials, both in CIH-exposed and sham rats (Table 2).

Renal excretory responses to VE

VE in CIH-exposed and sham rats resulted in significant increases in GFR, UF and Na^+ excretion (Figure 4d-g). The response pattern and magnitude of GFR and fractional Na^+ excretion during VE were similar in sham and CIH-exposed rats. Diuresis in response to VE was of significantly lesser magnitude in CIH-exposed rats compared with sham rats after 25 and 30 minutes (Figure 4d). Similarly, absolute Na^+ excretion was significantly less in CIH-exposed rats after 30 minutes of VE (Figure 4f). Analysis of AUC, reflecting the temporal cumulative response to VE, revealed that UF was significantly less in CIH-exposed rats compared with sham rats (Figure 4d, f).

RSNA response to VE

VE caused a progressive significant decrease in RSNA, which reached its maximum decline after 28-30 minutes (Figure 4c). The decrease in RSNA during VE with concomitant intra-renal infusion of saline was not significantly different in CIH-exposed and sham rats (Figure 4c).

High-pressure baroreflex

Representative recordings from high-pressure baroreflex trials are shown in Figure 5a. The slope of the RSNA baroreflex function curve of CIH-exposed rats was less than that of sham rats (A2 parameter: Figure 6a). This was related to a significant elevation in response range (A1 parameter) and operating range (Table 3) in CIH-exposed rats compared with sham rats. A rightward shift in the pressure at which the baroreceptors operate (A3 parameter), by ~20 mmHg ($p=0.005$), in CIH-exposed rats was observed (Figure 6 and Table 3).. Conversely, data from the second cohort study (with a more modest increase in MAP in CIH-exposed rats) revealed no difference in any of the parameters between CIH-exposed and sham rats (Figure 6).

These apparently conflicting results obtained from the two cohorts are likely explained by the moderate correlation (Figure 7) that we found between baseline blood pressure and the slope (A2, $R^2=0.386$, $p=0.017$) and mid-point pressure (A3, $R^2= 0.639$, $p<0.0001$) of RSNA baroreflex function curves, combining all rats in both cohorts. Parameters of the baroreflex control of HR were not significantly different between CIH-exposed and sham rats in either of the two cohort studies (Table 3).

Baseline MAP, HR, RSNA and renal excretory parameters during intra-renal TRPV1 blockade

Intra-renal infusion of saline had no significant effect on blood pressure, HR and RSNA in either cohort (Table 2 and Supplementary Table 1 https://figshare.com/s/7bc496e361e5e47043d7). In contrast, MAP was lower during intra-renal infusion of CPZ both in CIH-exposed and sham rats (of both cohorts), compared with

409 respective baseline values measured prior to CPZ infusion, whereas RSNA and HR were
410 unchanged (Table 2 and Supplementary Table 1
411 https://figshare.com/s/7bc496e361e5e47043d7). During intra-renal infusion of CPZ there
412 was a significant diuresis and natriuresis, both in CIH-exposed and sham rats compared with
413 respective values measured prior to CPZ infusion (Supplementary Table 2
414 https://figshare.com/s/7796b802afe6c02d54f0).

415

416 *Renal excretory responses to VE during intra-renal TRPV1 blockade*

417 During intra-renal infusion of CPZ, significant increases in UF and absolute Na^+
418 excretion in response to VE were observed in CIH-exposed and sham rats, with no significant
419 difference between the experimental groups (Figure 4).

420

421 *Low- and high-pressure baroreflex control during intra-renal TRPV1 blockade*

422 During intra-renal infusion of CPZ, the decrease in RSNA (% of max) in response to
423 VE was equivalent in CIH-exposed and sham rats (Figure 4c). However, an apparent
424 potentiation of the RSNA sympatho-inhibitory response to VE was observed in both groups
425 when RSNA (% of baseline) was considered (Supplementary Figure S1,
426 https://figshare.com/s/9659e62049b971e25ab7). Intra-renal CPZ did not significantly affect
427 high-pressure baroreflex of RSNA or HR in CIH-exposed and sham rats of cohort 2
428 (Supplementary Table 3 https://figshare.com/s/870e5f260f49995a4d8d, and Figure 6c and
429 6d).

430

431 *TRPV1 immunofluorescence in renal tissue*

432 TRPV1 channels are mainly expressed in the fibres located between the muscular
433 layer and the uroepithelium of the renal pelvic wall (Figure 8). Positive staining was also
434 expressed in the uroepithelium (Figure 8). TRPV1 fluorescence occupied 5.1±1.0% of the
435 area of the muscularis propria of the pelvic wall of CIH-exposed rats, which was equivalent
436 to sham rats (6.4±1.9%, Figure 8f). TRPV1 expression in the uroepithelium was equivalent
437 between CIH-exposed and sham rats (3.7±0.9% vs. 3.9±1.1%). TRPV1 protein concentration

in kidney tissue (Figure 8f, bottom) was not significantly different between CIH-exposed and sham rats.

Renal histopathological assessment

The average glomerular tuft area was equivalent in CIH-exposed and sham rats (Figure 9). A slightly greater degree of fibrosis was observed in the cortex of CIH-exposed kidneys compared with sham kidneys (Figure 9b and d). In contrast, there was no significant difference in collagen expression in the outer medulla between CIH-exposed and sham kidneys (Figure 9c and d).

Renal oxidative stress, inflammation and protein oxidation

The activity of NOX, SOD and catalase enzymes was measured in whole kidney tissue and there was no significant change in the activity of these enzymes after exposure to CIH. There was no significant difference in NOX, SOD and catalase enzyme activities between CIH-exposed and sham rats (Table 4). Furthermore, there was no evidence of greater protein oxidation in the kidneys of CIH-exposed rats (Table 4). Cytokine concentrations (IL-1β, keratinocyte chemoattractant/growth related oncogene and TNF-α) were not significantly different between CIH-exposed and sham rats (Table 4).

Discussion

This study provides several novel findings: 1) In CIH-exposed rats, diuretic and natriuretic responses to VE were impaired, notwithstanding that the sympatho-inhibitory response of RSNA to fluid overload was preserved; 2) the high-pressure baroreflex was modestly affected in CIH-exposed rats, an outcome that was related to the magnitude of CIH-induced hypertension, suggesting an indirect effect of exposure to CIH; 3) CIH-induced hypertension can manifest in the absence of renal injury.

VE produced reductions in RSNA similar to the findings of previous studies (8, 19). Exposure to CIH, sufficient to cause hypertension, did not adversely affect the sympatho-inhibitory response of RSNA to VE. This revealed that altered low-pressure baroreflex control of RSNA did not contribute to CIH-induced hypertension.

Basal renal function was equivalent in sham and CIH-exposed rats. However, the renal excretory response to VE in CIH-exposed rats was blunted with resultant sodium and fluid retention. These findings suggest that compensatory mechanisms in the kidney ensured maintenance of normal basal kidney function in the face of CIH-related stress and sympathetic over-activity. Dysfunction was revealed however, during VE challenge, with evidence of blunted diuretic and natriuretic responses, which appear independent of neural control of the kidney. Similarly, in streptozotocin-induced diabetic rats, basal diuresis and natriuresis were equivalent to non-diabetic rats, but excretory responses were impaired during VE (44). The underlying mechanisms that contribute to impairment of VE-dependent excretory responses are multifactorial and do not depend solely on changes in RSNA. Such mechanisms include alterations in renin-angiotensin system (RAAS) activity, renal perfusion pressure, and GFR. Thus, our finding of blunted sodium and fluid excretion during VE, despite preserved reflex reduction in RSNA, highlights that other mechanisms contribute to diuretic and natriuretic responses to VE and reveals that one or more of these mechanisms are perturbed by exposure to CIH.

Impaired cardiac baroreflex function was previously reported in people with OSA and in rats exposed to CIH (24, 38). Accordingly, we hypothesized that exposure to CIH disrupts the high-pressure baroreflex control of RSNA (3, 18, 20). CIH-exposed rats of the first cohort showed a significant shift in mid-point blood pressure by almost 20 mmHg, which was associated with an increase in the operating range of the RSNA baroreflex. Moreover, a

marked increase in response range (A1 parameter) of the RSNA baroreflex was evident in CIH-exposed rats. Elevation in the operating and response range of RSNA resulted in a decrease in the slope of the baroreflex (A2 parameter). These changes were concomitant with a substantial hypertensive phenotype (Table 1). Conversely, CIH-exposed rats of the second cohort with modest hypertension displayed baroreflex responsiveness that was equivalent to the respective sham group. Interestingly, a significant correlation between basal MAP and the baroreflex slope (A2) and between MAP and mid-point pressure (A3) was evident (Figure 7). This indicates that resetting of RSNA baroreflex and apparent decreased slope of the curve is associated with elevated blood pressure. It is likely that baroreflex adjustments following exposure to CIH in this study and marked attenuation of baroreflex function observed in severe CIH protocols, are secondary to the elaboration of hypertension following exposure to CIH, as the second cohort of rats were hypertensive (modest compared with cohort 1), but displayed no changes in baroreflex parameters revealing that the latter is not obligatory for the manifestation of CIH-induced hypertension.

The baroreflex control of HR was unchanged in CIH-exposed rats in agreement with previous studies utilizing 5, 7 and 10 days of exposure to CIH (24, 47, 50). Lai et al (24) analysed day-to-day arterial blood pressure and baroreflex sensitivity of the heart in conscious rats. MAP was higher by 15 mmHg after 5 days of exposure to CIH with no alteration in baroreflex function, followed by a decline in baroreflex sensitivity starting 10 days after the onset of exposure to CIH (24). Indeed, long-term exposure to CIH was associated with decreased cardiac baroreflex gain (11, 14, 27).

In renal injury, there is activation of renal pelvic chemoreceptors causing activation of afferent renal nerves, sympatho-excitation and hypertension (7, 23, 31, 34). In renal failure and high fat-induced obesity models, impairment of high- and low-pressure baroreflex function was linked to increased renal afferent nerve activity (3, 20). Therefore, renal denervation and/or suppression of renal inflammation is associated with restoration of the baroreflex control of RSNA (19, 21). Similarly, in some animal models of CIH, increases in systemic and renal inflammatory biomarkers and ROS have been reported together with impaired baroreflex control of HR (11, 24, 47). Afferent renal nerve fibres are abundant in the renal pelvic wall (23). A subset of these afferent nerves contains TRPV1, which is co-localized with neurotransmitters such as SP (17). In rats, cortico-medullary infusion of the TRPV1 agonist capsaicin induces an excitatory reno-renal reflex and an increase in blood pressure (36). It is also known that acute hypoxia increases the tonic activity of TRPV1

receptors. Hypoxia-induced activation of TRPV1 was suppressed using CPZ and Tiron, a membrane permeable ROS scavenger (22). Moreover, *in vitro* studies showed that TRPV1 activation decreases cell viability and induces apoptosis (42). This effect is mediated by an increase in intracellular calcium influx followed by ROS production, which causes mitochondrial depolarization and DNA fragmentation (42).

CPZ, at a similar dose to that used in the present study, was utilized in previous studies to block TRPV1 resulting in marked changes in RSNA (26). The infusion of CPZ over 30 minutes in the present study diffused into the pelvic wall where renal afferent nerves are located. This was confirmed histologically by observing the location of lissamine green stain infused for 30 minutes (not shown). Intra-renal infusion of CPZ caused a significant diuresis and natriuresis accompanied by significant reduction in MAP, but without an attendant decrease in RSNA. In addition, the renal sympatho-inhibitory response to VE after CPZ administration was unaffected, both in CIH-exposed and sham rats. Nevertheless, following intra-renal infusion of CPZ, diuretic and natriuretic responses to VE were equivalent in CIH-exposed and sham rats, which suggests a potential role of renal TRPV1 receptors in CIH-induced impairment of renal excretory function, although we cannot exclude the possibility that the intra-renal CPZ-induced diuresis and natriuresis per se (which was independent of RSNA) may have contributed to the recovery of renal excretory responses to VE in CIH-exposed rats, masking the original mechanism contributing to impaired renal excretory function. Therefore, our results should be viewed as preliminary and the molecular mechanisms contributing to CIH-induced impairment in renal excretory function requires further study.

Of interest, there was no difference between CIH-exposed and sham rats in TRPV1 expression in the renal pelvic wall. Histological analysis in the CIH-exposed rats showed modest cortical fibrosis, which may relate to decreased cortical oxygen tension and reduced renal blood flow in CIH-exposed rats, which was previously reported (32). Interestingly, neither inflammation nor altered pro- or anti-oxidant enzymatic activity was evident in CIH-exposed kidneys. Moreover, inflammatory cytokine concentrations were not different between experimental groups. Variable renal outcomes at the molecular level in animal models of CIH are likely related to differences in the pattern, duration and intensity of CIH, as recently reviewed (6). Glomerular hypertrophy and/or inflammation was reported in other studies (45), but were not observed in this study, suggesting that these changes, when they

occur, are more likely to be secondary to hypertension, rather than a direct effect of exposure to CIH, although they may also arise due to synergistic effects of hypertension and hypoxia.

This study has several limitations. Data were collected from anesthetized rat preparations. As such, cardiovascular, renal, and autonomic nervous system function were altered compared with the conscious state. It will be important to determine if exposure to CIH adversely affects renal excretory function in conscious animals. Intra-renal CPZ administration was unilateral, which might not reflect the full biological effect of TRPV1 antagonism. Unilateral infusion of drugs has been used effectively in other studies of baroreflex function (2, 3). In the present study, unilateral CPZ produced renal and cardiovascular effects, nevertheless the effects of bilateral TPRV1 inhibition is worthy of further investigation. For logistical reasons, high-pressure baroreflex function was not assessed after intra-renal CPZ in rats of cohort 1, where baroreflex alterations were subsequently revealed. The effect of intra-renal CPZ was assessed in rats of cohort 2, but high-pressure baroreflex control of RSNA was preserved in these rats with modest hypertension. Therefore, we cannot discount a possible role for TRPV1 signalling in modulating high-pressure baroreflex control of RSNA in CIH-exposed rats and this warrants further attention. Our study design involved the assessment of RSNA and renal excretory responses to VE in successive challenges, before and after intra-renal TRPV1 blockade. We acknowledge that restoration of renal excretory responses to VE in CIH-exposed rats, which was attributed to blockade of TRPV1 receptors, might relate to the performance of a second VE trial per se, independent of antagonism. Moreover, renal excretory responses to the second VE challenge should be viewed in the context of the profound diuresis and natriuresis caused by intra-renal CPZ. Our data on GFR during VE should be viewed cautiously given that measurements were not taken in steady-state conditions and blood sampling was limited as we did not wish to interfere with MAP, and hence reflex control of RSNA, during VE challenges.

In summary, a relatively modest paradigm of exposure to CIH was sufficient to induce hypertension, without evidence of renal inflammation and/or oxidative stress. Exposure to CIH blunted sodium and fluid excretion in response to VE with preserved suppression of RSNA. Exposure to CIH induced modest changes in high-pressure baroreflex control of RSNA, which was dependent on the magnitude of blood pressure elevation in CIH-exposed rats suggesting that modulation of high-pressure baroreflex control of RSNA in this model is a consequence of hypertension, but may in turn proceed to a pathological level and

contribute to disease progression. Our results suggest that exposure to CIH causes renal dysfunction, which may be relevant to obstructive sleep apnea.

Acknowledgements: We are grateful for technical support provided by Dr Greg Jasionek, Department of Physiology, UCC and Dr Kieran Rea, APC Microbiome Centre, Ireland. We are thankful for the support with imaging provided by Dr Suzanne Crotty, Department of Anatomy & Neuroscience, UCC. We also acknowledge staff of the Biological Services Unit, UCC for support in the maintenance and welfare of animals used in the study.

Funding: Sara AlMarabeh was in receipt of a scholarship from the University of Jordan to support her doctoral training. The study was funded by the Department of Physiology, UCC.

Conflict of interest: The authors declare no conflict of interest.

References

1. **Abdel-Kader K, Dohar S, Shah N, Jhamb M, Reis SE, Strollo P, Buysse D, and Unruh ML**. Resistant hypertension and obstructive sleep apnea in the setting of kidney disease. *J Hypertens* 30: 960-966, 2012.

2. **Abdulla MH, Brenan N, Ryan E, Sweeney L, Manning J, and Johns EJ**. Tacrolimus restores the high and low-pressure baroreflex control of renal sympathetic nerve activity in cisplatin-induced renal injury rats. *Exp Physiol* 104: 1726-1736, 2019.

3. **Abdulla MH, Duff M, Swanton H, and Johns EJ**. Bradykinin receptor blockade restores the baroreflex control of renal sympathetic nerve activity in cisplatin-induced renal failure rats. *Acta Physiol (Oxf)* 218: 212-224, 2016.

4. **Abuyassin B, Badran M, Ayas NT, and Laher I**. Intermittent hypoxia causes histological kidney damage and increases growth factor expression in a mouse model of obstructive sleep apnea. *PLoS One* 13: e0192084, 2018.

5. **Adeseun GA, and Rosas SE**. The impact of obstructive sleep apnea on chronic kidney disease. *Curr Hypertens Rep* 12: 378-383, 2010.

6. **AlMarabeh S, Abdulla MH, and O'Halloran KD**. Is Aberrant Reno-Renal Reflex Control of Blood Pressure a Contributor to Chronic Intermittent Hypoxia-Induced Hypertension? *Front Physiol* 10: 465, 2019.

7. **Banek CT, Knuepfer MM, Foss JD, Fiege JK, Asirvatham-Jeyaraj N, Van Helden D, Shimizu Y, and Osborn JW**. Resting Afferent Renal Nerve Discharge and Renal Inflammation: Elucidating the Role of Afferent and Efferent Renal Nerves in Deoxycorticosterone Acetate Salt Hypertension. *Hypertension* 68: 1415-1423, 2016.

8. **Buckley MM, and Johns EJ**. Impact of L-NAME on the cardiopulmonary reflex in cardiac hypertrophy. *Am J Physiol Regul Integr Comp Physiol* 301: R1549-1556, 2011.

9. **Campese VM, and Kogosov E**. Renal afferent denervation prevents hypertension in rats with chronic renal failure. *Hypertension* 25: 878-882, 1995.

10. **Dalmasso C, Jacqueline LR, Mounce S, Xu X, and Anglia LS**. Capsaicin-Induced Stimulation of Sensory Neurons in Adipose Tissue Promotes Increases in Blood Pressure in Mice Exposed to Early Life Stress. *FASEB* 574.11: 2019.

11. **Del Rio R, Andrade DC, Lucero C, Arias P, and Iturriaga R**. Carotid Body Ablation Abrogates Hypertension and Autonomic Alterations Induced by Intermittent Hypoxia in Rats. *Hypertension* 68: 436-445, 2016.

12. **Foss JD, Wainford RD, Engeland WC, Fink GD, and Osborn JW**. A novel method of selective ablation of afferent renal nerves by periaxonal application of capsaicin. *Am J Physiol Regul Integr Comp Physiol* 308: R112-122, 2015.

13. **Gontijo JR, and Kopp UC**. Renal sensory receptor activation by calcitonin gene-related peptide. *Hypertension* 23: 1063-1067, 1994.

14. **Gu H, Lin M, Liu J, Gozal D, Scrogin KE, Wurster R, Chapleau MW, Ma X, and Cheng ZJ**. Selective impairment of central mediation of baroreflex in anesthetized young adult Fischer 344 rats after chronic intermittent hypoxia. *Am J Physiol Heart Circ Physiol* 293: H2809-2818, 2007.

15. **Hart EC, and Charkoudian N**. Sympathetic neural regulation of blood pressure: influences of sex and aging. *Physiology (Bethesda)* 29: 8-15, 2014.

16. **Kario K, Bhatt DL, Kandzari DE, Brar S, Flack JM, Gilbert C, Oparil S, Robbins M, Townsend RR, and Bakris G**. Impact of Renal Denervation on Patients With Obstructive Sleep Apnea and Resistant Hypertension - Insights From the SYMPLICITY HTN-3 Trial. *Circ J* 80: 1404-1412, 2016.

17. **Kassmann M, Harteneck C, Zhu Z, Nürnberg B, Tepel M, and Gollasch M**. Transient receptor potential vanilloid 1 (TRPV1), TRPV4, and the kidney. *Acta Physiol (Oxf)* 207: 546-564, 2013.

18. **Kaur M, Chandran DS, Jaryal AK, Bhowmik D, Agarwal SK, and Deepak KK**. Baroreflex dysfunction in chronic kidney disease. *World J Nephrol* 5: 53-65, 2016.

19. **Khan SA, Sattar MA, Rathore HA, Abdulla MH, Ud Din Ahmad F, Ahmad A, Afzal S, Abdullah NA, and Johns EJ**. Renal denervation restores the baroreflex control of renal sympathetic nerve activity and heart rate in Wistar-Kyoto rats with cisplatin-induced renal failure. *Acta Physiol (Oxf)* 210: 690-700, 2014.

20. **Khan SA, Sattar MZ, Abdullah NA, Rathore HA, Abdulla MH, Ahmad A, and Johns EJ**. Obesity depresses baroreflex control of renal sympathetic nerve activity and heart rate in Sprague Dawley rats: role of the renal innervation. *Acta Physiol (Oxf)* 214: 390-401, 2015.

21. **Khan SA, Sattar MZA, Abdullah NA, Rathore HA, Ahmad A, Abdulla MH, and Johns EJ**. Improvement in baroreflex control of renal sympathetic nerve activity in obese Sprague Dawley rats following immunosuppression. *Acta Physiol (Oxf)* 221: 250-265, 2017.

22. **Kim KS, Yoo HY, Park KS, Kim JK, Zhang YH, and Kim SJ**. Differential effects of acute hypoxia on the activation of TRPV1 by capsaicin and acidic pH. *J Physiol Sci* 62: 93-103, 2012.

23. **Kopp UC**. Role of renal sensory nerves in physiological and pathophysiological conditions. *Am J Physiol Regul Integr Comp Physiol* 308: R79-95, 2015.

24. **Lai CJ, Yang CC, Hsu YY, Lin YN, and Kuo TB**. Enhanced sympathetic outflow and decreased baroreflex sensitivity are associated with intermittent hypoxia-induced systemic hypertension in conscious rats. *J Appl Physiol (1985)* 100: 1974-1982, 2006.

676 25. **Leuenberger UA, Brubaker D, Quraishi SA, Quraishi S, Hogeman CS, Imadojemu VA,**
677 **and Gray KS**. Effects of intermittent hypoxia on sympathetic activity and blood pressure in humans.
678 *Auton Neurosci* 121: 87-93, 2005.
679 26. **Li J, and Wang DH**. Differential mechanisms mediating depressor and diuretic effects of
680 anandamide. *J Hypertens* 24: 2271-2276, 2006.
681 27. **Lin M, Liu R, Gozal D, Wead WB, Chapleau MW, Wurster R, and Cheng ZJ**. Chronic
682 intermittent hypoxia impairs baroreflex control of heart rate but enhances heart rate responses to vagal
683 efferent stimulation in anesthetized mice. *Am J Physiol Heart Circ Physiol* 293: H997-1006, 2007.
684 28. **Lu W, Kang J, Hu K, Tang S, Zhou X, Xu L, Li Y, and Yu S**. The role of the Nox4-
685 derived ROS-mediated RhoA/Rho kinase pathway in rat hypertension induced by chronic intermittent
686 hypoxia. *Sleep Breath* 21: 667-677, 2017.
687 29. **Lu W, Kang J, Hu K, Tang S, Zhou X, Yu S, and Xu L**. Angiotensin-(1-7) relieved renal
688 injury induced by chronic intermittent hypoxia in rats by reducing inflammation, oxidative stress and
689 fibrosis. *Braz J Med Biol Res* 50: e5594, 2017.
690 30. **Marfurt CF, and Echtenkamp SF**. Sensory innervation of the rat kidney and ureter as
691 revealed by the anterograde transport of wheat germ agglutinin-horseradish peroxidase (WGA-HRP)
692 from dorsal root ganglia. *J Comp Neurol* 311: 389-404, 1991.
693 31. **Nishi EE, Bergamaschi CT, and Campos RR**. The crosstalk between the kidney and the
694 central nervous system: the role of renal nerves in blood pressure regulation. *Exp Physiol* 100: 479-
695 484, 2015.
696 32. **O'Neill J, Jasionek G, Drummond SE, Brett O, Lucking EF, Abdulla MA, and**
697 **O'Halloran KD**. Renal cortical oxygen tension is decreased following exposure to long-term but not
698 short-term intermittent hypoxia in the rat. *Am J Physiol Renal Physiol* 316: F635-F645, 2019.
699 33. **Oga Y, Saku K, Nishikawa T, Kishi T, Tobushi T, Hosokawa K, Tohyama T, Sakamoto**
700 **T, Sunagawa K, and Tsutsui H**. The impact of volume loading-induced low pressure baroreflex
701 activation on arterial baroreflex-controlled sympathetic arterial pressure regulation in normal rats.
702 *Physiol Rep* 6: e13887, 2018.

703 34. **Patel KP, Xu B, Liu X, Sharma NM, and Zheng H**. Renal Denervation Improves
704 Exaggerated Sympathoexcitation in Rats With Heart Failure: A Role for Neuronal Nitric Oxide
705 Synthase in the Paraventricular Nucleus. *Hypertension* 68: 175-184, 2016.
706 35. **Prabhakar NR, and Kumar GK**. Mechanisms of sympathetic activation and blood pressure
707 elevation by intermittent hypoxia. *Respir Physiol Neurobiol* 174: 156-161, 2010.
708 36. **Qiu Y, Zheng F, Ye C, Chen AD, Wang JJ, Chen Q, Li YH, Kang YM, and Zhu GQ**.
709 Angiotensin Type 1 Receptors and Superoxide Anion Production in Hypothalamic Paraventricular
710 Nucleus Contribute to Capsaicin-Induced Excitatory Renal Reflex and Sympathetic Activation.
711 *Neurosci Bull* 36: 463-474, 2020.
712 37. **Ramchandra R, and Barrett CJ**. Regulation of the renal sympathetic nerves in heart failure.
713 *Front Physiol* 6: 238, 2015.
714 38. **Resta O, Guido P, Rana L, Procacci V, Scarpelli F, and Picca V**. Depressed baroreceptor
715 reflex in patients with obstructive sleep apnea (OSA). *Boll Soc Ital Biol Sper* 72: 247-254, 1996.
716 39. **Ribon-Demars A, Pialoux V, Boreau A, Marcouiller F, Larivière R, Bairam A, and**
717 **Joseph V**. Protective roles of estradiol against vascular oxidative stress in ovariectomized female rats
718 exposed to normoxia or intermittent hypoxia. *Acta Physiol (Oxf)* 225: e13159, 2018.
719 40. **Sharpe AL, Calderon AS, Andrade MA, Cunningham JT, Mifflin SW, and Toney GM**.
720 Chronic intermittent hypoxia increases sympathetic control of blood pressure: role of neuronal
721 activity in the hypothalamic paraventricular nucleus. *Am J Physiol Heart Circ Physiol* 305: H1772-
722 1780, 2013.
723 41. **Silva AQ, and Schreihofer AM**. Altered sympathetic reflexes and vascular reactivity in rats
724 after exposure to chronic intermittent hypoxia. *J Physiol* 589: 1463-1476, 2011.
725 42. **Sun Z, Han J, Zhao W, Zhang Y, Wang S, Ye L, Liu T, and Zheng L**. TRPV1 activation
726 exacerbates hypoxia/reoxygenation-induced apoptosis in H9C2 cells via calcium overload and
727 mitochondrial dysfunction. *Int J Mol Sci* 15: 18362-18380, 2014.
728 43. **Witkowski A, Prejbisz A, Florczak E, Kądziela J, Śliwiński P, Bieleń P, Michałowska I,**
729 **Kabat M, Warchoł E, Januszewicz M, Narkiewicz K, Somers VK, Sobotka PA, and Januszewicz**

730 **A**. Effects of renal sympathetic denervation on blood pressure, sleep apnea course, and glycemic
731 control in patients with resistant hypertension and sleep apnea. *Hypertension* 58: 559-565, 2011.
732 44. **Wongmekiat O, and Johns E**. Contribution of endothelial nitric oxide synthase in the
733 blunted renal responses to volume expansion in diabetic rats. *Exp Physiol* 86: 481-488, 2001.
734 45. **Wu X, Chang SC, Jin J, Gu W, and Li S**. NLRP3 inflammasome mediates chronic
735 intermittent hypoxia-induced renal injury implication of the microRNA-155/FOXO3a signaling
736 pathway. *J Cell Physiol* 233: 9404-9415, 2018.
737 46. **Wu X, Gu W, Lu H, Liu C, Yu B, Xu H, Tang Y, Li S, Zhou J, and Shao C**. Soluble
738 Receptor for Advanced Glycation End Product Ameliorates Chronic Intermittent Hypoxia Induced
739 Renal Injury, Inflammation, and Apoptosis via P38/JNK Signaling Pathways. *Oxid Med Cell Longev*
740 2016: 1015390, 2016.
741 47. **Yamamoto K, Eubank W, Franzke M, and Mifflin S**. Resetting of the sympathetic
742 baroreflex is associated with the onset of hypertension during chronic intermittent hypoxia. *Auton*
743 *Neurosci* 173: 22-27, 2013.
744 48. **Zhang Y, Su X, Zou F, Xu T, Pan P, and Hu C**. Toll-like receptor-4 deficiency alleviates
745 chronic intermittent hypoxia-induced renal injury, inflammation, and fibrosis. *Sleep Breath* 23: 503-
746 513, 2018.
747 49. **Zhao MM, Tan XX, Ding N, and Zhang XL**. [Comparison of efficacy between continuous
748 positive airway pressure and renal artery sympathetic denervation by radiofrequency ablation in
749 obstructive sleep apnea syndrome patients with hypertension]. *Zhonghua Yi Xue Za Zhi* 93: 1234-
750 1237, 2013.
751 50. **Zoccal DB, Bonagamba LG, Paton JF, and Machado BH**. Sympathetic-mediated
752 hypertension of awake juvenile rats submitted to chronic intermittent hypoxia is not linked to
753 baroreflex dysfunction. *Exp Physiol* 94: 972-983, 2009.
754 51. **Zoccal DB, Simms AE, Bonagamba LG, Braga VA, Pickering AE, Paton JF, and**
755 **Machado BH**. Increased sympathetic outflow in juvenile rats submitted to chronic intermittent
756 hypoxia correlates with enhanced expiratory activity. *J Physiol* 586: 3253-3265, 2008.

Figure legends:

Figure 1: A schematic representation of the experimental protocol. In sham and CIH-exposed rats of cohort 1, following a 1 hour stabilization period, baseline cardiovascular and RSNA were determined. After intra-renal infusion of saline to the left kidney for 30 minutes, phenylephrine (PE, 50 µg/ml, 0.2 ml) and sodium nitroprusside (SNP, 50 µg/ml, 0.2 ml) were infused intravenously to elicit high-pressure baroreflex responses. The first volume expansion (VE) trial (saline phase) was then performed, which was followed by a 90-minute recovery period. Then, intra-renal infusion of CPZ was initiated for 30 minutes into the left kidney and a second VE trial was performed. Two urine samples (U1 and U2) were collected during baseline before each VE trial. The "Urine collection" phase represents the collection of a urine sample 10 minutes after the start of the VE trial followed by subsequent collection of urine samples every 5 minutes until the end of the VE challenge. Arterial blood was sampled for plasma (P1 and P2). Each VE trial was accompanied by infusion of inulin (FITC-inulin in saline, 10 mg/kg) for 30 minutes via the femoral vein at 0.25 ml/min/100g body weight using a syringe pump (Graseby syringe pump 8100, Dublin, Ireland). Each VE trial period was followed by 30 minutes of recovery during which infusion of saline through the intravenous line was stopped, but with continuous intra-renal infusion of saline or CPZ. P, plasma sample; VE, volume expansion; I.R., intra-renal; CPZ, capsaizepine; PE, phenylephrine; SNP, sodium nitroprusside.

Figure 2: Assessment of renal fibrosis. A virtual grid was used for the random selection of kidney regions. Sirius red stained images were converted to grey scale and a colour threshold function was used to highlight collagen labelling in red.

785 **Figure 3: Original recordings of cardiovascular parameters and RSNA in an**
786 **anesthetised rat.** Representative original recordings of baseline arterial pressure (AP), heart
787 rate (HR) which was derived from the AP recording, and raw and integrated RSNA (Int.
788 RSNA) recordings from a sham rat.
789
790 **Figure 4: Cardiovascular, RSNA and renal excretory responses to VE.** In sham (n=8) and
791 CIH-exposed rats (n=9), MAP, HR, RSNA, UF, GFR, absolute and fractional Na^+ excretion
792 responses to VE challenges were determined. In the left-hand panels, the time course of
793 responses to and recovery from VE during intra-renal infusion of saline or CPZ (TRPV1
794 blocker) are shown. Data (mean±SE) were averaged over each 2-minute period during VE
795 trials. Two-way ANOVA (time x exposure) was used to statistically compare the data. #
796 $p<0.05$ for time; Φ $p<0.05$ for time points significantly different from respective baseline
797 (post-hoc analysis); Ψ $p<0.05$ for exposure; * $p<0.05$ compared with corresponding time
798 point in sham rats. In the right-hand panels, area under the curve (AUC) analysis for the
799 respective responses is shown (expressed in arbitrary units, AU), calculated using the
800 trapezoidal rule, by the summation of the VE period. Data are shown as individual data points
801 for each rat, with box and whiskers plots representing the interquartile range and maximum
802 and minimum values. Data were compared with independent *t*-tests. Significance was taken
803 at $p<0.0125$, accounting for multiple comparisons. MAP, mean arterial pressure; RSNA,
804 renal sympathetic nerve activity; UF, Urine flow; GFR, glomerular filtration rate; MAP,
805 mean arterial blood pressure; HR, heart rate; CPZ, capsaizepine.
806
807 **Figure 5: Original recordings illustrating high- and low-pressure baroreflex control of**
808 **RSNA in anesthetised rats.** Representative original recordings of arterial blood pressure,
809 raw and integrated RSNA responsiveness to blood pressure manipulations evoking the high-
810 pressure baroreflex (a) and VE evoking the low-pressure baroreflex (b). Recordings are
811 shown for representative sham and CIH-exposed rats showing responses during intra-renal
812 infusion of saline and intra-renal infusion of CPZ, (TRPV1 blocker). AP, arterial blood
813 pressure; RSNA, renal sympathetic nerve activity; Int. RSNA, integrated RSNA; VE, volume
814 expansion; CPZ, capsaizepine.
815

816 **Figure 6: High-pressure baroreflex control of RSNA.** Data (mean±SE) are shown for
817 RSNA (% of baseline) as a function of arterial blood pressure in sham and CIH-exposed rats
818 of the first (a; sham, n=10; CIH, n=8) and second cohort (b; sham, n=10; CIH, n=10). In
819 graphs (c) and (d), data (mean±SE) are shown for RSNA (% of baseline) as a function of
820 arterial blood pressure during intra-renal infusion of saline and CPZ (TRPV1 blocker) of
821 sham (c) and CIH-exposed rats (d) of the second cohort. Data for baroreflex parameters are
822 shown in table 3 and supplementary table 3 (https://figshare.com/s/870e5f260f49995a4d8d).
823 RSNA, renal sympathetic nerve activity; BP, blood pressure.

824

825 **Figure 7: Correlations between baseline MAP and baroreflex parameters.** The
826 relationship between mean arterial blood pressure and the baroreflex parameters, A3 and A2,
827 are shown for all sham (n=20) and CIH-exposed rats (n=18). Linear regression analysis was
828 performed. Significance was taken at $P<0.05$. MAP, mean arterial blood pressure; A3,
829 midpoint pressure of the response; A2, gain coefficient.

830

831 **Figure 8: TRPV1 immunofluorescence in the renal pelvic wall.** Immunofluorescence
832 labeling of renal pelvic wall showing TRPV1-positive labeling within the muscularis propria
833 (white arrows) and uroepithelium layer (red arrows). (a) is a representative image from a
834 sham kidney and (b) is a representative image from a CIH-exposed kidney. Negative controls
835 demonstrate specificity of the antibodies used in the study (c, primary antibody omitted; e,
836 secondary antibody omitted); Blue labelling of nuclei by Hoescht. (d) Immunofluorescence
837 labeling of TRPV1 channels in neuronal cell bodies of lumbar dorsal root ganglia as a
838 positive control. Scale bar 50 µm. Data for TRPV1-positive staining (% of total area) in sham
839 (n=8) and CIH-exposed rats (n=9) are shown as individual data points for each rat, and box
840 and whiskers plots representing the interquartile range and maximum and minimum values (f,
841 top). Data for TRPV1 protein concentration of kidney tissue homogenate in sham (n=12) and
842 CIH-exposed rats (n=8) are shown as individual data points for each rat, with box and
843 whiskers plots representing the interquartile range and maximum and minimum values (f,
844 bottom). Data were compared with independent *t*-tests. Significance was taken at $p<0.05$.

845

Figure 9: Renal histology. Representative images from a sham and CIH-exposed rat are shown. (a) shows hematoxylin and eosin staining; (b) shows Sirius red staining of renal cortex; (c) shows Sirius red staining of renal outer medulla. Scale bar 50 μm. Data for glomerular tuft area and percentage fibrotic area are presented in (d) as individual data points for each rat, with box and whiskers plots representing the interquartile range and maximum and minimum values. Data from sham (n=8) and CIH-exposed rats (n=8) were compared using independent *t*-tests. Significance was taken at $p<0.05$.

Figure 1

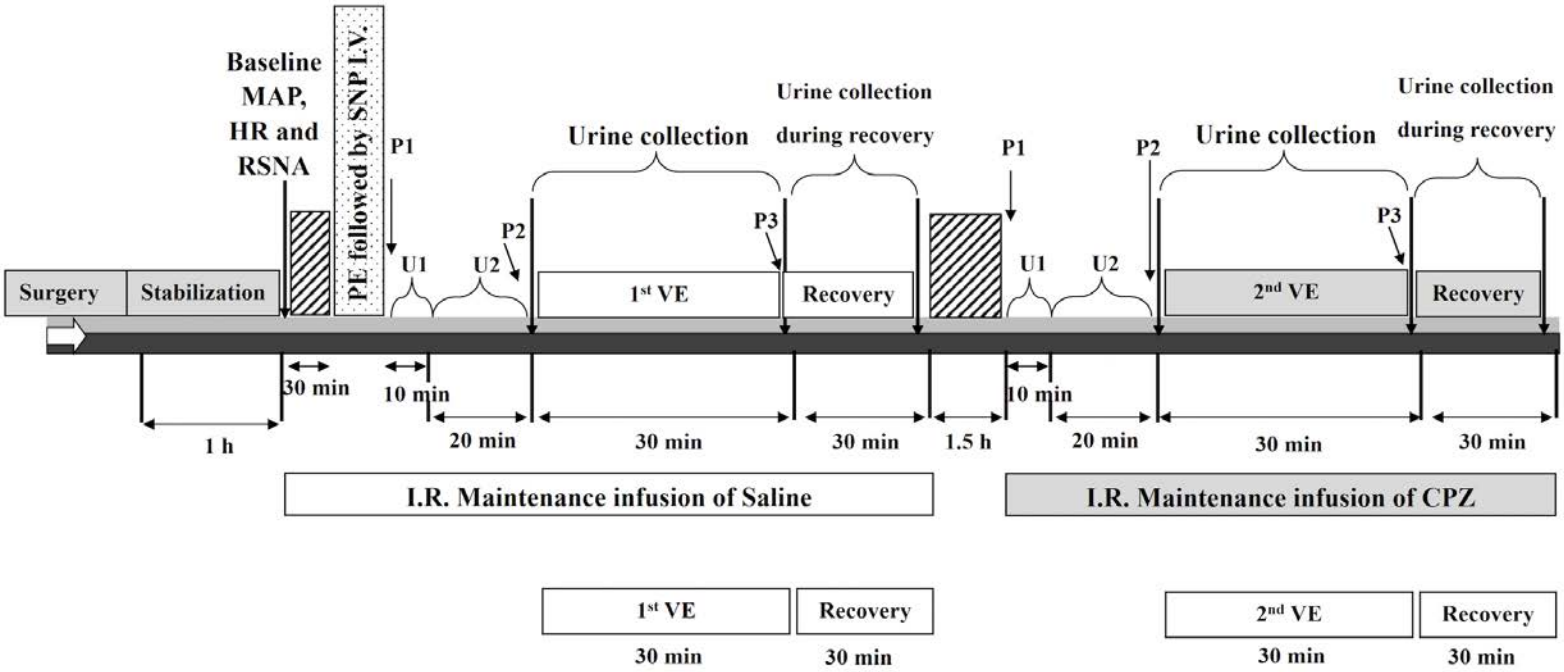

Figure 2

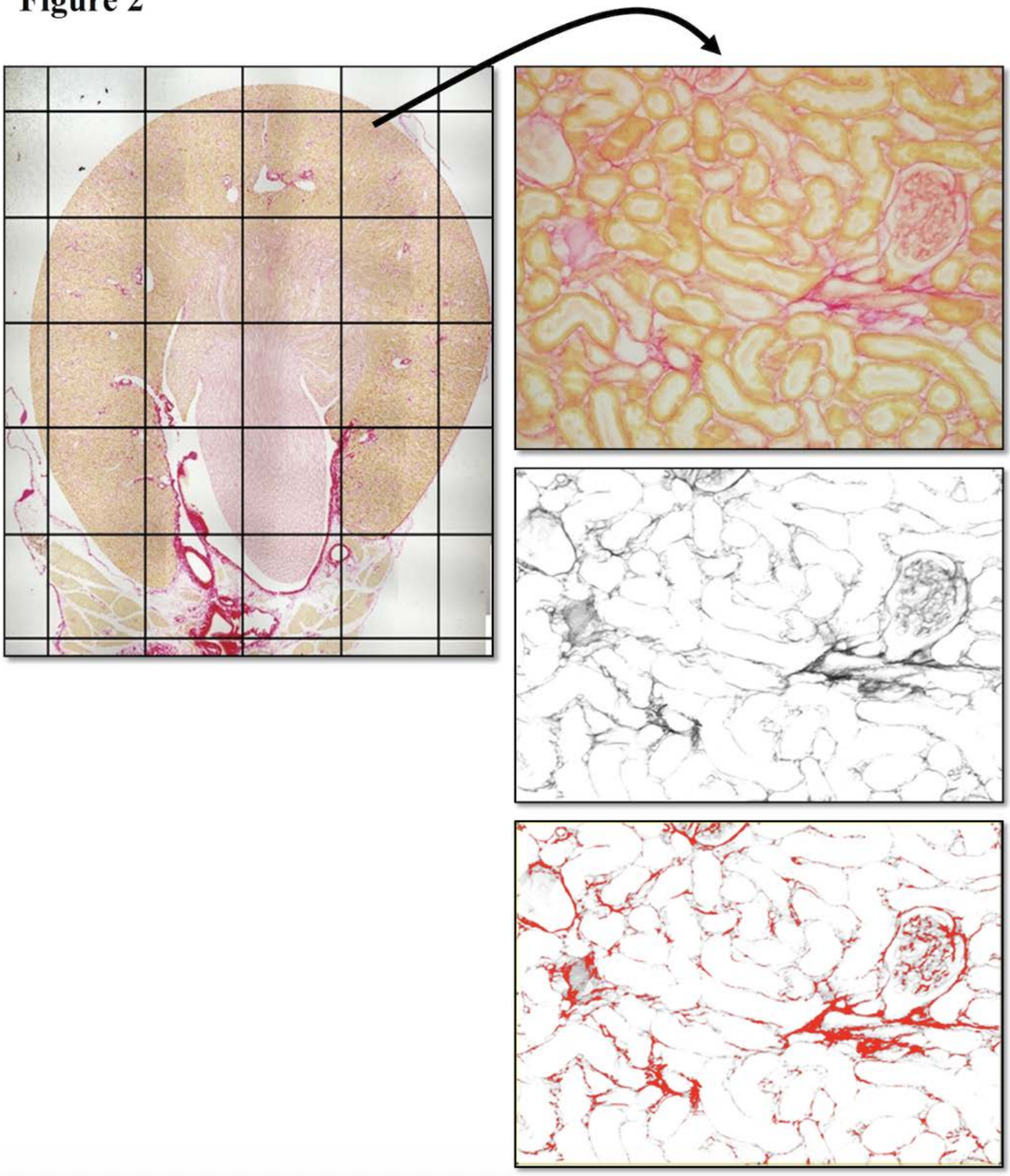

Figure 3

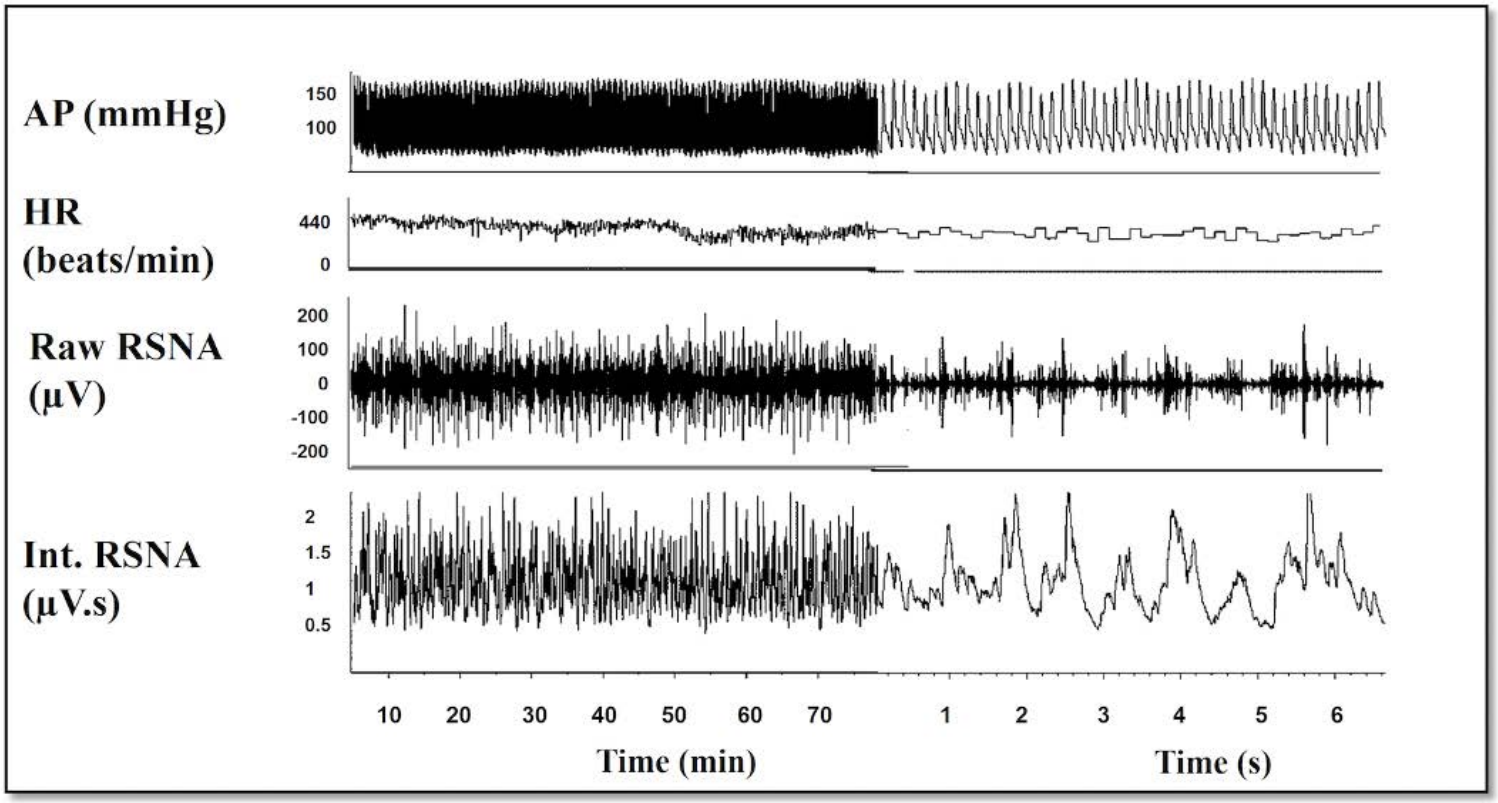

Figure 4

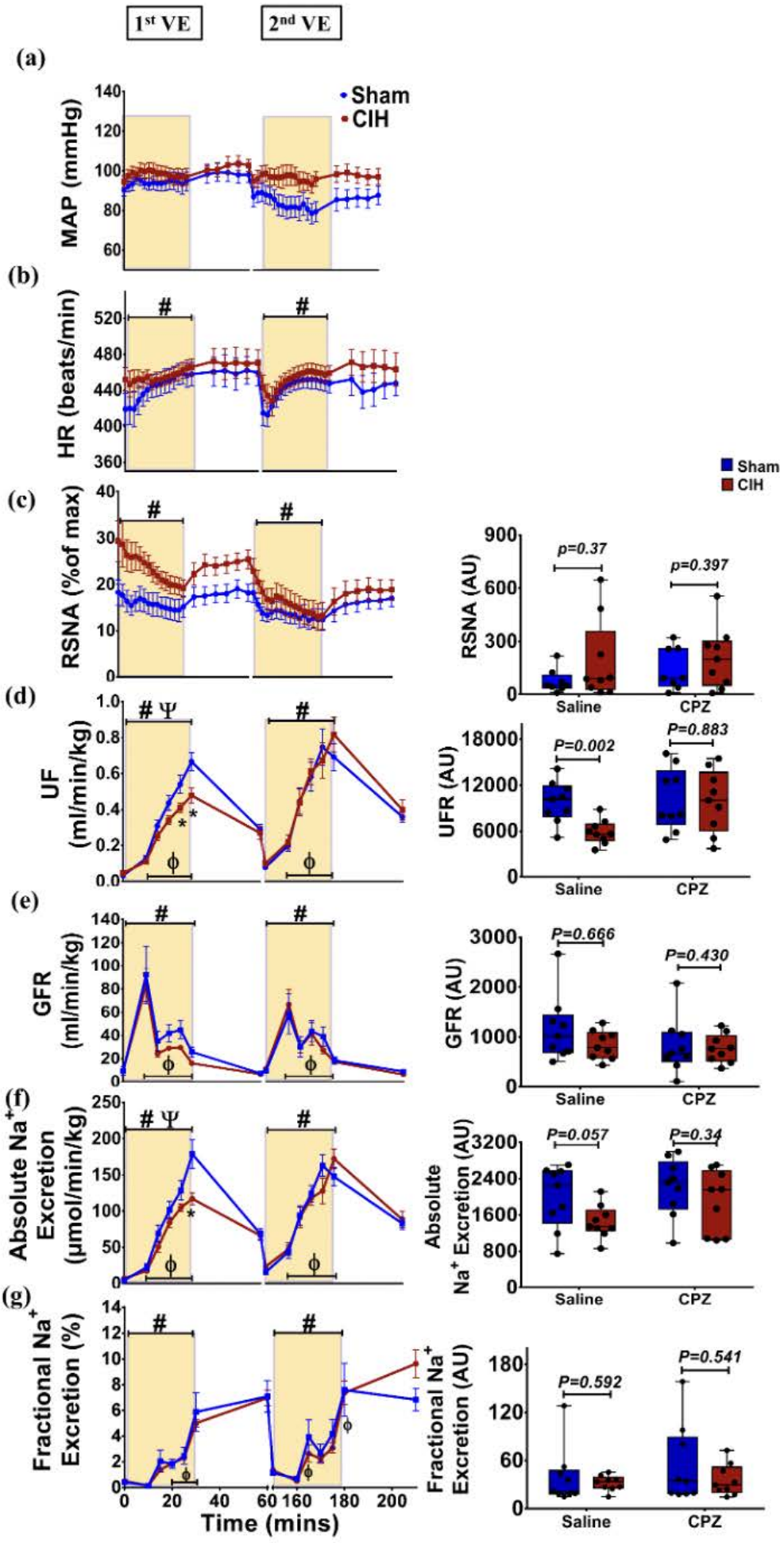

Figure 5

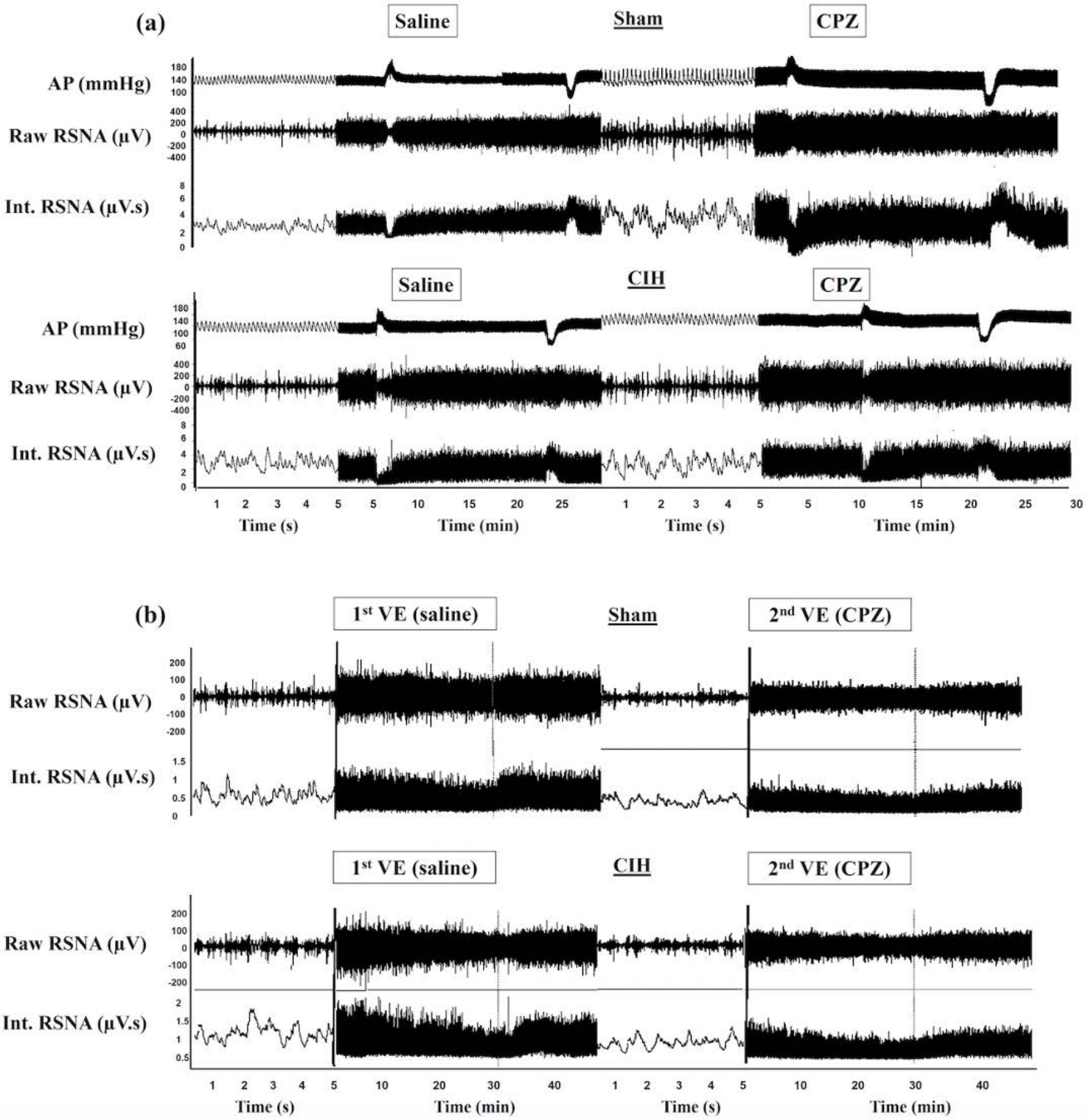

Figure 6

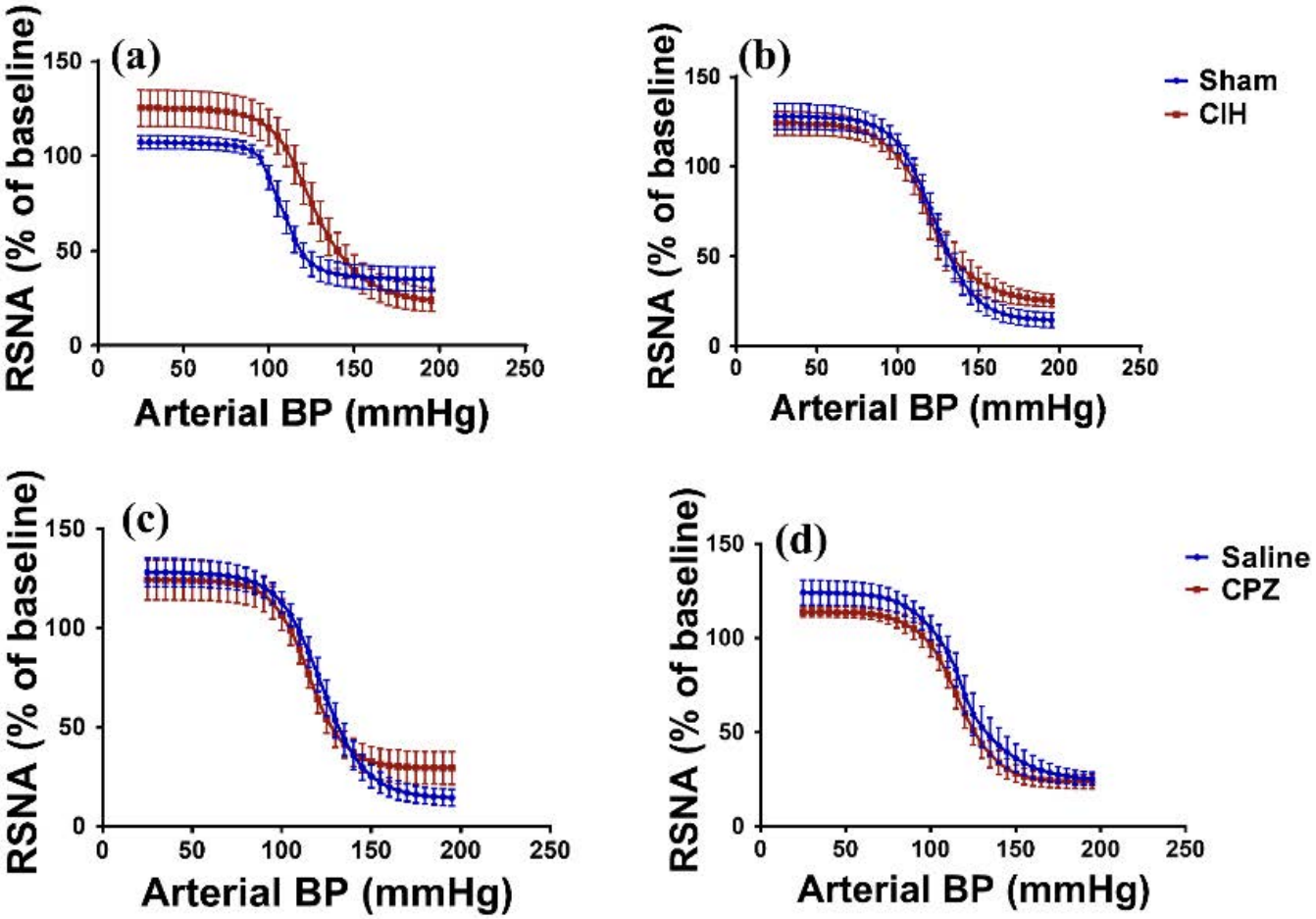

Figure 7

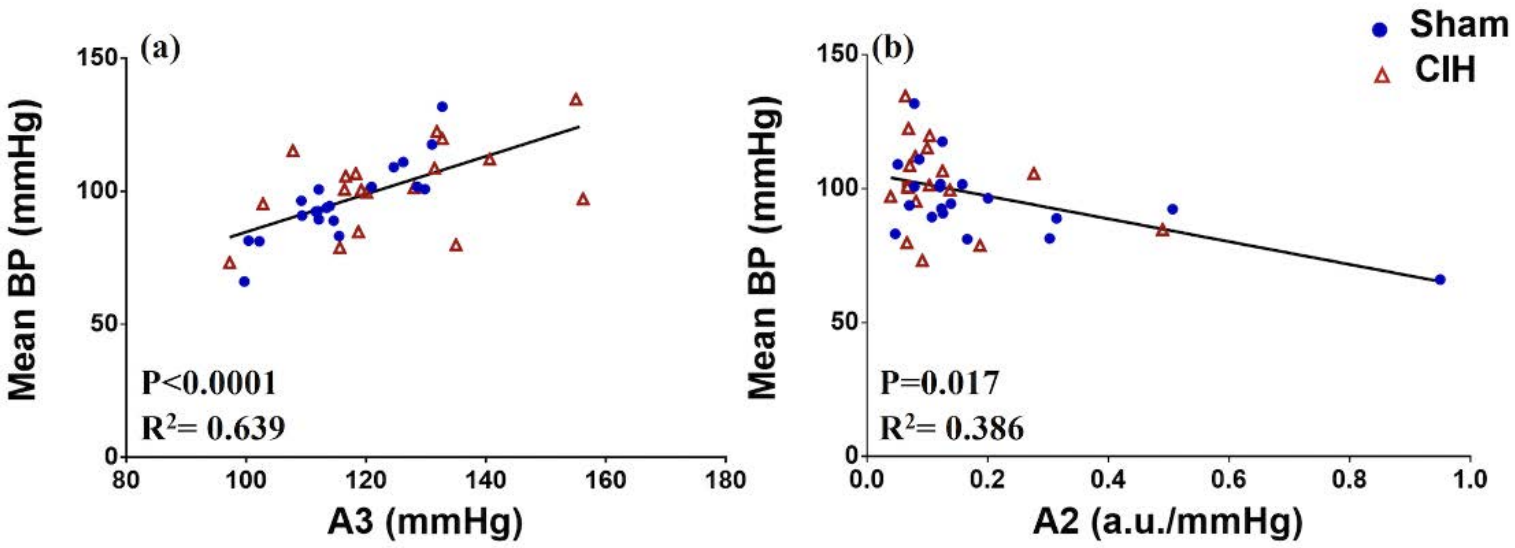

Figure 8

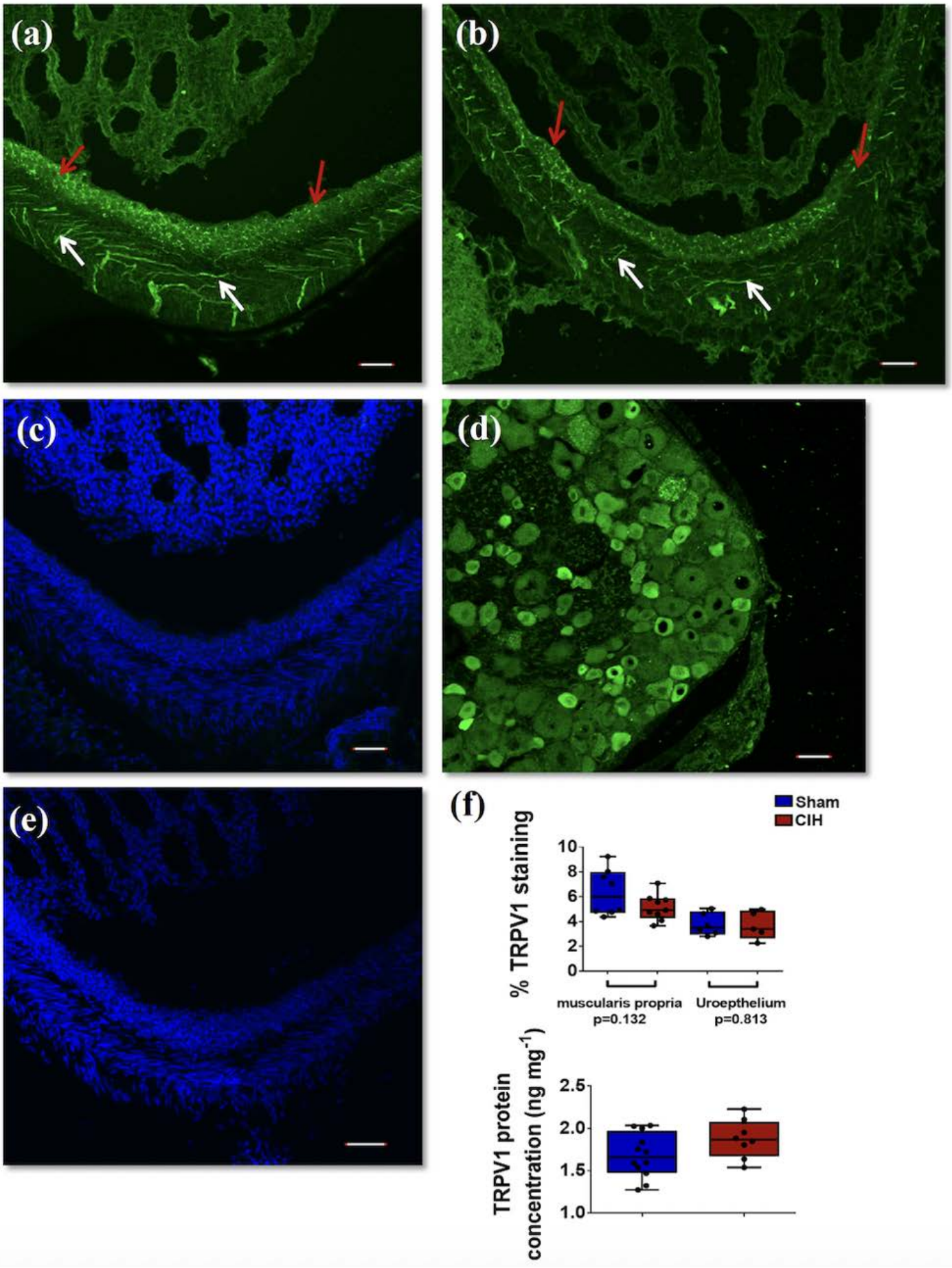

Figure 9

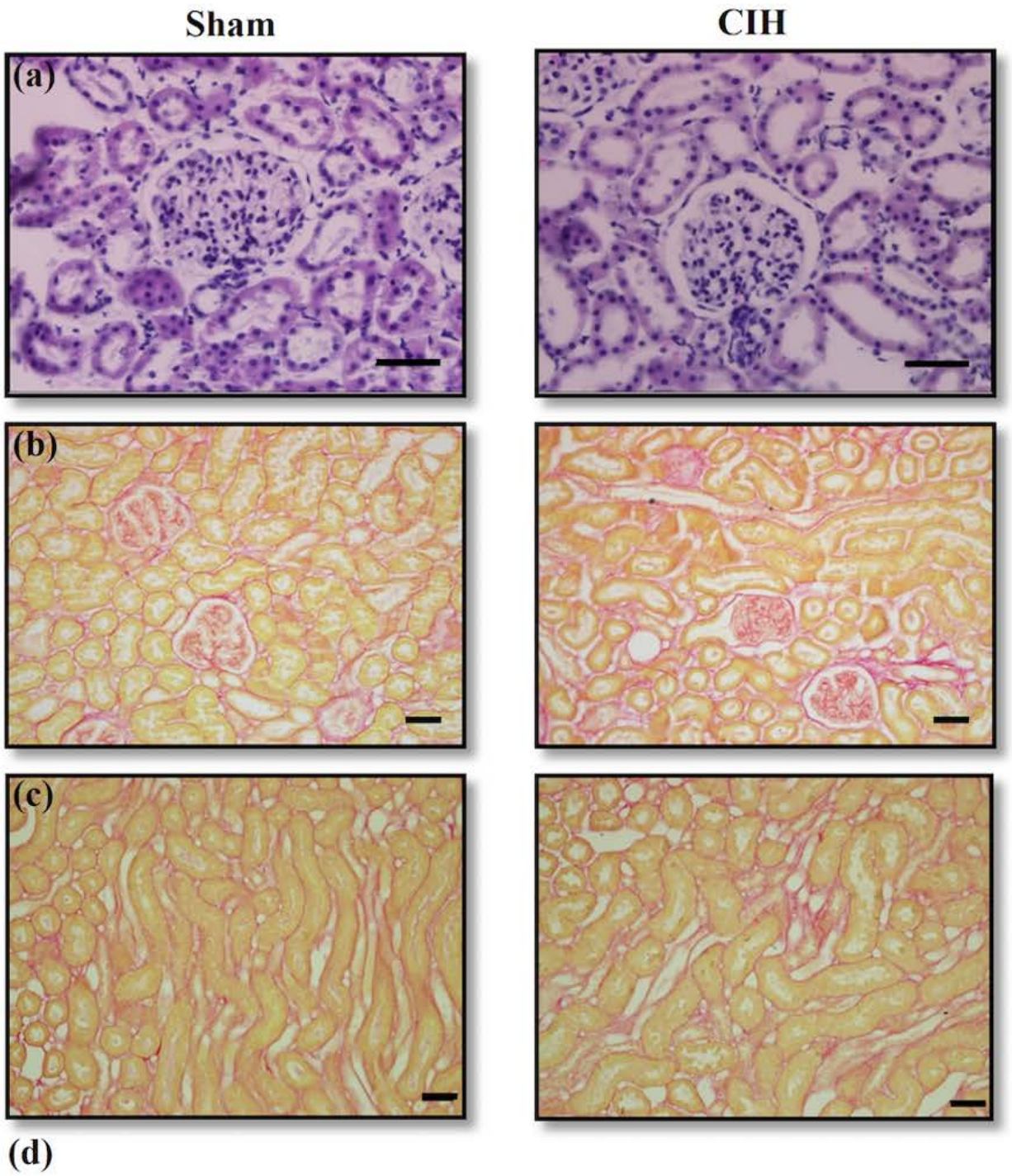

Table 1. Baseline cardiovascular and RSNA parameters in sham and CIH-exposed rats

Parameter	Sham	CIH	p-value	Sham	CIH	p-value
After arterial cannulation (before renal surgical instrumentation)						
	First cohort			*Second cohort*		
MAP (mmHg)	124±13	143±7*	**0.001**	115±11	127±9*	**0.014**
SBP (mmHg)	143±17	163±11*	**0.008**	137±13	144±12	0.154
DBP (mmHg)	114±12	133±5*	**<0.0001**	104±11	118±10*	**0.005**
HR (beats/min)	432±28	461±39	0.083	411±29	425±41	0.355
After stabilization (after renal surgical instrumentation)						
MAP (mmHg)	84±9	97±11*	**0.028**	103±12	107±18	0.565
SBP (mmHg)	116±14	125±15	0.262	134±15	132±22	0.871
DBP (mmHg)	69±8	82±11*	**0.043**	88±13	94±19	0.365
HR (beats/min)	400±52	445±47	0.084	436±19	450±34	0.204
RSNA (% of max)	17±7	36±15*	**0.006**	24±10	32±18	0.387
RSNA (uV.s)	0.66±0.30	1.34±0.73	0.231	1.39±0.84	1.67±0.65	0.878
Maximum RSNA (uV .s)	4.70±2.03	4.03±2.18	0.349	7.04±5.29	6.60±3.54	1.000

Data are presented as mean±SD and were collected from the first (sham, n=10; CIH-exposed, n=9) and second cohorts of animals (sham, n=13; CIH, n=10). Baseline cardiovascular parameters were recorded for 2 minutes ~4-5 minutes after arterial cannulation i.e. before retroperitoneal incisions were performed to expose the kidneys. Cardiovascular parameters and RSNA were also recorded for 2 minutes after the stabilization period, 1 hour following renal surgical instrumentation. Parameters were analysed using independent samples t-test or Mann-Whitney test. * $p<0.05$ between exposure groups. CIH, chronic intermittent hypoxia; MAP, mean arterial blood pressure; SBP, systolic blood pressure; DBP, diastolic blood pressure; HR, heart rate; RSNA (% of max), renal sympathetic nerve activity normalized to maximum activity recorded during baroreflex activation during euthanasia.

Table 2. MAP, HR and RSNA before and during VE challenges in sham and CIH-exposed rats.

	First VE (saline phase)				Second VE (CPZ phase)			
Parameter	MAP (mmHg)	HR (beats/min)	RSNA (% of max)	RSNA (uV.s)	MAP (mmHg)	HR (beats/min)	RSNA (% of max)	RSNA (uV.s)
	Before intra-renal infusion of saline				*Before intra-renal infusion of CPZ*			
Sham	90±9	409±35	15±5	0.71±0.34	94±11	430± 41	18±6	0.87±0.43
CIH	99±10	444±49	32±18$^{\phi}$	1.19±0.82	98±11	448± 42	23±6	0.95±0.72
	After intra-renal saline (before VE)				*After intra-renal CPZ (before VE)*			
Sham	90±8	408±49	18±8	0.86±0.50	83±5$^{\#}$	412±45	18±6	0.86±0.41
CIH	90±4	428±46	30±14$^{\phi}$	1.14±0.78	90±5$^{\#}$	431±46	22±8	0.94±0.74
	Last two minutes of VE				*Last two minutes of VE*			
Sham	92±15	451±35*	15±6*		76±10	443±33*	12±6*	
CIH	91±9	458±31*	18±5*		90±9	450±25*	11±8*	
	2x2 ANOVA (before vs. after intra-renal saline/CPZ)							
Exposure	P=0.075	P=0.131	**P=0.035**	P=0.180	P=0.225	P=0.165	P=0.158	P=0.567
Time	P=0.102	P=0.084	P=0.894	P=0.330	**P=0.024**	P=0.100	P=0.722	P=0.396
Exposure x time	P=0.065	**P=0.007**	**P=0.044**	P=0.137	P=0.502	P=0.748	P=0.975	P=0.838
	2x2 ANOVA (after intra-renal saline/CPZ vs. last two minutes of VE)							
Exposure	P=0.516	P=0.404	P=0.077		P=0.045	P=0.205	P=0.581	
Time	P=0.072	**P<0.001**	**P=0.01**		P=0.168	**P=0.002**	**P=0.001**	
Exposure x time	P=0.786	P=0.182	P=0.115		P=0.073	P=0.218	P=0.252	

Data were collected from sham (n=8) and CIH-exposed rats (n=9) of the first cohort. Data are expressed as mean±SD. Baseline values over a 2-minute period were averaged before and after the infusion of saline or CPZ and were analysed using repeated-measures two-way ANOVA. The last two minutes of each VE trial were averaged and compared with baseline values collected immediately before VE using repeated-measures two-way ANOVA. * $p<0.05$ vs. corresponding value after intra-renal infusion of saline/drug. $^{\#}$

31 $p<0.05$ vs. corresponding value before intra-renal infusion of drug. $^{\phi}$ $p<0.05$ vs. sham.
32 MAP, mean arterial blood pressure; HR, heart rate; VE, volume expansion; CPZ,
33 capsaizepine; RSNA (% of max), renal sympathetic nerve activity normalized to
34 maximum activity recorded during baroreflex activation during euthanasia.

35

36

37

Table 3. High-pressure baroreflex parameters during intra-renal infusion of saline in sham and CIH-exposed rats (cohort 1 and cohort 2).

Parameter	**Sham**	**CIH**	**p-value**	**Sham**	**CIH**	**p-value**
RSNA baroreflex						
	First cohort			*Second cohort*		
A1 (%)	73±26	104±32*	**0.043**	114±30	100±22	0.280
A2 ($mmHg^{-1}$)	0.29±0.27	0.09±0.05*	**0.016**	0.10±0.03	0.15±0.14	0.912
A3 (mmHg)	109±6	129±14*	**0.005**	123±8	121±17	0.757
A4 (%)	35±20	22±13	0.131	14±13	24±10	0.062
Max. gain ($mmHg^{-1}$)	5.0±4.9	2.4±1.3	0.237	2.8±0.9	3.4±2.5	0.739
Operating range (mmHg)	27±23	53±25*	**0.016**	44±16	40±18	0.646
HR baroreflex						
	First cohort			*Second cohort*		
A1 (beats/min)	59±25	65±44	0.732	88±31	92±40	0.843
A2 ($mmHg^{-1}$)	0.16±0.18	0.19±0.19	0.673	0.12±0.08	0.11±0.04	0.674
A3 (mmHg)	116±9	122±15	0.341	125±17	125±15	0.999
A4 (beats/min)	370±46	410±59	0.139	387±38	397±76	0.707
Max. gain ($mmHg^{-1}$)	1.8±1.5	2.1±1.5	0.423	2.2±0.8	2.2±0.9	0.821

Data are expressed as mean±SD and represent baroreflex parameters of cohort 1 (sham, n=10; CIH, n=8) and cohort 2 (sham, n=10; CIH, n=10). Datawere analysed using independent sample *t*-tests. * $p<0.05$ vs. sham group. CIH, chronic intermittent hypoxia; RSNA, renal sympathetic nerve activity; HR, heart rate; A1, response range of RSNA/HR; A2, the gain coefficient; A3, midpoint pressure of input; A4, the minimum response.

Table 4: Biomarker concentrations in kidney tissue homogenates of sham and CIH-exposed rats.

Parameter	Sham	CIH	p-value
AOPP (μM)	15.6±2.2 (n=12)	14.8±3.1 (n=8)	0.728
NADPH oxidase activity (mU/min)	3.54±0.87 (n=8)	4.37±1.27 (n=9)	0.167
SOD activity (U/ml)	803.5±125.0 (n=11)	792.3±120.8 (n=8)	0.846
Catalase activity (U/ml)	15939±2888 (n=12)	17448±2539 (n=8)	0.105
TNF-α (pg/mg)	0.22±0.22 (n=8)	0.16±0.14 (n=10)	0.790
IL-1β (pg/mg)	5.04±1.34 (n=11)	6.15±1.31 (n=10)	0.070
Keratinocyte chemoattractant/growth related oncogene (pg/mg)	1.59±0.55 (n=11)	1.98±0.78 (n=9)	0.137

Data are expressed as mean±SD. AOPP, advanced oxidation protein products; SOD, superoxide dismutase. SOD activity, keratinocyte chemoattractant/growth related oncogene and IL-1β concentrations were analysed using independent samples *t*-test. Other biomarkers were analysed using Mann-Whitney test.

Chronic intermittent hypoxia impairs diuretic and natriuretic responses to volume expansion in rats with preserved low-pressure baroreflex control of the kidney

METHODS

Male Wistar rats
In hypoxia chambers

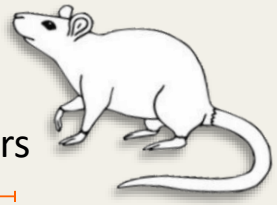

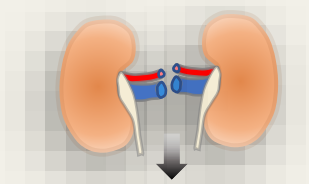

Sodium and water excretion

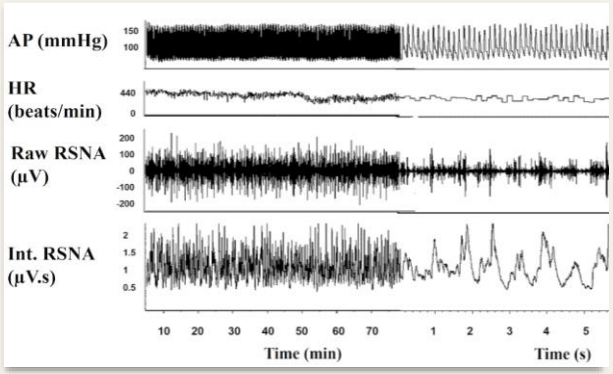

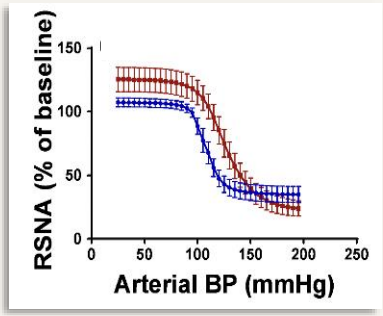

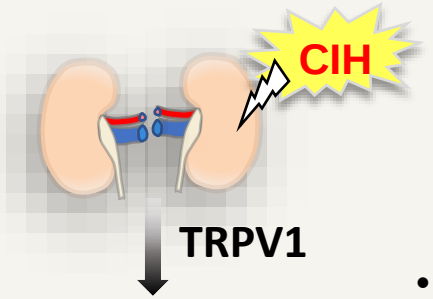

Impaired natriuresis and diuresis

OUTCOME

- RSNA High-pressure Baroreflex sensitivity ↓
- Mid-point blood pressure ↑

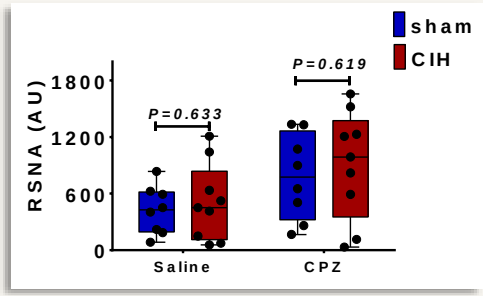

- Low-pressure baroreflex control of RSNA ↔

CONCLUSION

Exposure to CIH blunts the high-pressure but not low-pressure baroreflex control of RSNA, most likely indirectly due to hypertension. CIH also impairs diuretic and natriuretic responses to fluid overload, which may involve intra-renal TRPV1 signaling.

F-00377-2020